Charles University

Faculty of Mathematics and Physics

HABILITATION THESIS

Petr Dohnal

State Selectivity in Recombination of Molecular Ions with Electrons

Department of Surface and Plasma Science

Prague 2022

"If you can meet with Triumph and Disaster

And treat those two impostors just the same"

Kipling

Acknowledgements

Contents

Introduction

This thesis summarizes many years of experimental studies focused on recombination of atomic and molecular ions with electrons. Gradually, my scientific interest shifted from binary and third-body assisted recombination processes to question of different reactivity of different quantum states of molecular ions.

The presented experiments were performed using various modifications of stationary afterglow (SA-CRDS, Cryo-SA-CRDS) and flowing afterglow with Langmuir probe (Cryo-FALP II) techniques.

The thesis consists of several chapters. The first chapter (Theoretical background) introduces various recombination processes and covers basics of used absorption spectroscopy, Langmuir probe and microwave diagnostics. The second chapter (Experimental techniques) gives overview of instrumentation used for electron – ion recombination studies and the third chapter (Results) covers the most important results of my studies. The last chapter summarizes the thesis and is followed by a list of publications with me as author or co-author. Attached to this thesis are some of my publications that provide detailed information on the topics discussed in the text.

I have also collaborated on several experiments focused on the study of reactions of ions with molecules in 22-pole radiofrequency ion trap apparatus. As I was not, with some exceptions, main investigator in these studies, I decided to include into this thesis only two examples of how the trapping technique can be effectively utilized to distinguish between two isomers of the same mass or to probe internal excitation of trapped ions.

Theoretical background

Recombination of positive ions with electrons

Mutual neutralization of electron – positive ion system in cold plasmas can be governed by several mechanisms. These will be covered in the following sections. An important distinguishing factor is if the collision involves only electron and the cation – binary processes (radiative and dielectronic recombination, dissociative recombination) or if a collision with another particle is necessary to finish the recombination (third-body assisted recombination). The former processes will be important in low density environments such as the interstellar gas clouds whereas the latter will dominate at high ambient gas or electron number densities, especially at very low temperatures.

Radiative and dielectronic recombination

In low density environments the atomic ions A^+ can recombine with electrons e^- by radiative recombination. In this case, the stabilization of the neutral excited complex formed in recombination proceeds via emission of radiation:

$$A^+ + e^- \rightarrow h\nu,\tag{1}$$

here h is the Planck constant and ν is the frequency of emitted radiation.

Another possible process at such conditions is dielectronic recombination [*Schippers et al.*, 2010], where the excess energy is taken away by excitation of one of the bounded electrons of the ion to another bounded orbit. This is then followed a photon emission. Due to the discrete electronic energies this is a strongly energy dependent resonant process. The typical recombination rate coefficients are on the order of 10^{-9} cm^3s^{-1} or less at 300 K.

Dissociative recombination

For molecular ions, the electron – positive ion system formed during recombination can get rid of the excess energy by dissociating in to neutral fragments. Dissociative recombination, first proposed by Bates [*Bates et al.*, 1947] as an effective loss process for electrons in Earth's ionosphere, can proceed via different mechanisms and may involve many highly excited Rydberg states of the neutral molecule.

Motivated by contemporary afterglow studies on plasma deionization [*Biondi et al.*, 1949a; *Biondi et al.*, 1949b], Bates has shown in his seminal paper [*Bates*, 1950] that recombination of molecular ions with electrons can proceed very fast with rate coefficients on the order of 10^{-7} cm^{3}s^{-1}. According to Bates [*Bates*, 1950], the electron colliding with the ion is captured into a neutral dissociating state (the state is doubly excited with respect to the original ion – electron system) and this is followed by dissociation of the molecule in to neutral fragments. The described process is now known as direct dissociative recombination and its schematic representation is shown in Figure 1.
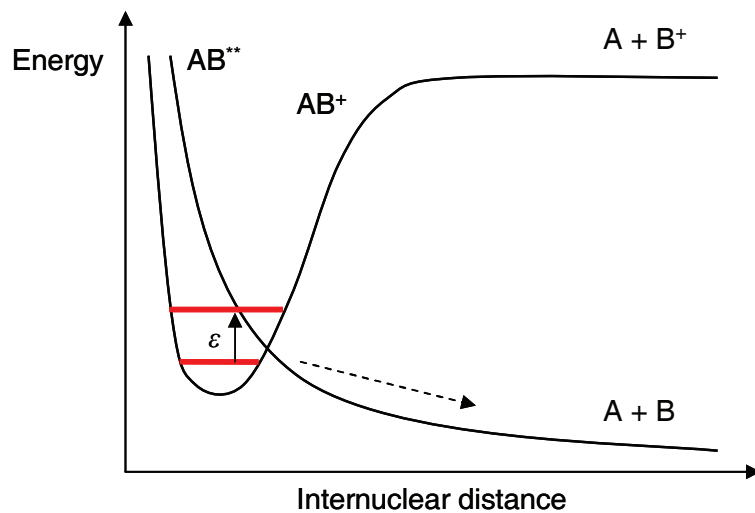
Figure 1. Adapted from refs. [*Larsson et al.,* 2008; *Dohnal*, 2013]. The potential energy curve of the ion, denoted AB$^+$, is crossed by the dissociative resonant state AB**. In the direct process of dissociative recombination, the capture of the incoming electron (with kinetic energy ε) in the resonant state is followed by dissociation on the potential energy curve.

In the direct dissociative recombination, the favourable curve crossing between the ionic and the resonant state is a necessary prerequisite for fast recombination process. Later, Bardsley [*Bardsley*, 1968] proposed a modification of Bates' mechanism, for cases in which the incoming electron cannot be directly captured into the resonant dissociating state. Instead, it is captured into a vibrational state of one of the infinite series of Rydberg states of the neutral converging to the ionic state. After that, it couples to the resonant dissociating state and finally the dissociation of the molecule occurs. This indirect process of dissociative recombination is depicted in Figure 2.
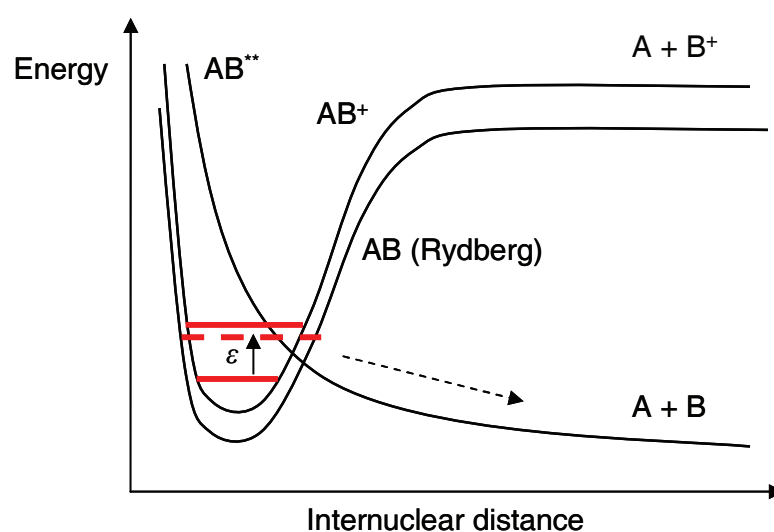
Figure 2. Adapted from refs. [*Larsson et al.,* 2008; *Dohnal*, 2013]. Indirect dissociative recombination process.

Other mechanisms were proposed such as recombination involving core-excited resonances [*Guberman*, 1995] or direct predissociation [Guberman, 1994]. For further details I refer the reader to the excellent book on dissociative recombination by Larsson and Orel [*Larsson et al.,* 2008].

Recombination assisted by third particle

At conditions typical for low temperature afterglow recombination studies (electron temperature close to 300 K, electron number density below 10^{10} cm^{-3} with buffer gas number densities on the order of 10^{17} cm^{-3} or below) the influence of third bodies on the overall measured recombination rate coefficient can be usually neglected. At enhanced gas or electron number densities or at very low temperature, the third body assisted processes can substantially contribute to plasma deionization.

In electron assisted collisional recombination (E-CRR) the excess energy of the formed electron – ion metastable neutral complex is taken away in collision(s) with electron(s):

$$A^+ + e^- + e^- \xrightarrow{K_{E-CRR}} A + e^-, \tag{2}$$
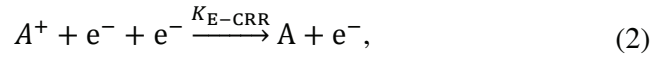
Where K_{E-CRR} is the ternary recombination rate coefficient of E-CRR. According to semi-classical theoretical studies [*Bates et al.*, 1962; *Mansbach et al.*, 1969; *Stevefelt et al.*, 1975], multiple collisions are necessary for stabilisation of ion – electron collisional complex. An analytical formula for the effective binary recombination rate coefficient α_{E-CRR} as a result of E-CRR of atomic ions was derived by Stevefelt [*Stevefelt et al.*, 1975]:

$$\alpha_{E-CRR} = 3.8 \times 10^{-9} T_e^{-4.5} n_e + 1.55 \times 10^{-10} T_e^{-0.63} +$$
$$6 \times 10^{-9} T_e^{-2.18} n_e^{0.37} \text{ cm}^3\text{s}^{-1}, \tag{3}$$

where electron number density n_e is in units of cm^{-3} and electron temperature T_e is in Kelvins. According to ref. [*Stevefelt et al.*, 1975] the first term in equation (3) accounts for collisional recombination, the radiative processes give rise to the second term and the third term describes coupling between collisional and radiative recombination. Due to its steep temperature dependence, the first term in equation (3) dominates at low temperatures. The corresponding ternary recombination rate coefficient K_{E-CRR} is then:

$$K_{E-CRR} = \frac{\alpha_{E-CRR}}{n_e} \cong 3.8 \times 10^{-9} T_e^{-4.5} \text{ cm}^6\text{s}^{-1}, \tag{4}$$

where n_e and T_e are in units of cm^{-3} and K, respectively.

Later theoretical treatment by Pohl [*Pohl et al.*, 2008] suggested slightly lower value of the pre-factor in equation (4) – 2.77×10^{-9} K$^{4.5}$ cm^{6}s^{-1}. The values of $K_{E\text{-}CRR}$ that me and my co-workers obtained for Ar$^+$ ions in the temperature range of 60 – 150 K [*Kotrík et al.*, 2011a; *Kotrík et al.*, 2011b; *Dohnal et al.*, 2013] are within error of the measurement in agreement with both of these predictions [*Stevefelt et al.*, 1975; *Pohl et al.*, 2008] but closer to the values given by equation (3).

E-CRR is considered an important process in formation of antihydrogen [*Killian et al.*, 1999; *Pohl et al.*, 2008; *Wolz et al.*, 2020] and it was discussed in connection with cold and ultracold plasmas [*Rennick et al.*, 2011]. There are many theoretical and numerical simulation studies [*Bannash et al., 2011*; *Vorob'ev*, 2017; *Gerber*, 2018; *Jiang et al.*, 2020] with emphasis on low temperature E-CRR but the vast majority of available experimental data was obtained at electron temperature of 300 K or higher [*Mansbach et al.*, 1969; *Berlande et al.*, 1970; *Curry*, 1970; *Skrzypkowski et al.*, 2004]. To the best of my knowledge, the only direct measurement of E-CRR recombination rate coefficient in plasma for electron temperatures below 300 K are the CRYO-FALP II studies focused on Ar$^+$ ions [*Kotrík et al.*, 2011a; *Kotrík et al.*, 2011b; *Dohnal et al.*, 2013]. There is no experimental or theoretical study concerning E-CRR of molecular ions. Recent experiments [*Hejduk et al.*, 2015] suggest that for some molecular ions the value of the E-CRR rate coefficient may be substantially lower than for atomic ones.

If the particle that carries away the excess energy of recombination is neutral we will call this process neutral assisted collisional radiative recombination (N-CRR):

$$A^+ + e^- + M \xrightarrow{K_{N\text{-}CRR}} A + M .$$
(5)

N-CRR of atomic ions has been studied theoretically from early 20th century [*Thomson*, 1924; *Pitaevskii*, 1962; *Flannery*, 1991; *Wojcik et al.*, 1999; *Wojcik et al.*, 2000]. The recombination rate coefficient is predicted to depend steeply on temperature as ~ $T^{-2.5}$ [*Thomson*, 1924; *Pitaevskii*, 1962] or ~ $T^{-2.9}$ [*Bates et al.*, 1965].

The experimental studies of N-CRR performed for atomic ions or He$_2^+$ largely agree with theoretical predictions [*Berlande et al.*, 1970; *Deloche et al.*, 1976; *Gousset et al.*, 1978; *Sonsbeek et al.*, 1992; *Schregel et al.*, 2016]. There are only very few

studies performed for temperatures below 300 K. Cao et al. [*Cao et al.*, 1991] studied N-CRR for mixture of atmospheric ions in helium obtaining good agreement with theory. Me and my co-workers have investigated the recombination of Ar^+ with electrons in ambient helium [*Dohnal et al.*, 2013] with results very close to theoretical predictions [*Bates et al.*, 1965].

In 2008 Glosik et al. [*Glosik et al.*, 2008] discovered a very fast helium assisted recombination of H_3^+ ions with ternary recombination rate coefficient on the order of 10^{-25} cm^6s^{-1}, i. e. more than hundred times higher than what would have been expected based on the theory of Bates and Khare [*Bates et al.*, 1965]. We later observed similar behaviour for the deuterated isotopologues of H_3^+ [*Dohnal et al.*, 2012c; *Dohnal et al.*, 2016; *Plašil et al.*, 2017].

The explanation suggested in ref. [*Glosík et al.*, 2009] assumed that after collision of H_3^+ ions with electrons a Rydberg state with a long life-time is formed. The Rydberg state then lives long enough to experience *l*-changing collision with helium facilitating the recombination process. This was supported by calculations by C. Greene and V. Kokoouline of lifetimes of Rydberg states formed in H_3^+ recombination. The explanation was successful in predicting the order of magnitude of the ternary recombination rate coefficient but rested on some crude assumptions especially for the rate of *l*-changing collisions between H_3 Rydberg states and helium. Moreover, similar mechanism could be expected also for other molecular ions recombining via indirect recombination process involving Rydberg states. Our studies on HCO^+ [*Korolov et al.*, 2009] and N_2H^+ [*Shapko et al.*, 2020] recombination in helium buffer gas have shown that the values of the corresponding ternary recombination rate coefficients are at least order of magnitude lower than those for H_3^+ ions.

Absoption spectroscopy

Basic concepts

Absorption of radiation by a quantum system is connected with a transition between two energy levels. The decrease of the intensity I of monochromatic light passing through homogenous absorbing medium is given by the Lambert-Beer law [*Beer*, 1852]:

$$\frac{dI(x,v)}{dx} = -\alpha(v)I(x,v),$$

(6)

where x is the position in the absorbing medium, v is the frequency of the radiation and $\alpha(v)$ is absorption coefficient. In homogenous absorbing medium, α does not depend on x and the solution of equation (6) is:

$$I(L,v) = I_0 \exp(-\alpha(v)L),$$

(7)

where L is the distance traversed in the absorbing medium and I_0 is the initial light intensity. Absorption coefficient depends on the number density of the absorbing medium $N(x)$ and on the photo-absorption cross-section $\sigma(v)$:

$$\alpha(x,v) = N(x)\sigma(v).$$

(8)

The shape of the absorption line is given by the line-shape function $g(v)$:

$$\sigma(v) = Sg(v),$$

(9)

where S stands for integral absorption coefficient (line intensity).

Absorbance:

$$A(v) = -\ln\left(\frac{I(v)}{I_0(v)}\right),$$

(10)

connects measured quantities with absorption coefficient. By substituting (7) in to equation (10) we get:

$$A(v) = \alpha(v)L.$$

(11)

In a more general case of non-homogenous absorbing medium containing more than one absorbing specie, the absorbance is given by:

$$A(\nu) = \sum_j \sigma_j(\nu) \int_0^L N_j(x)\mathrm{d}x \,, \qquad (12)$$

Where σ_j is the phot-absorption cross section of a specie with number density $N_j(x)$.

Spectral line broadening

Several processes can influence the line-shape function $g(\nu)$ of measured absorption line. At experimental conditions for studies covered in this thesis, the most important are: lifetime broadening, collisional broadening and Doppler broadening.

The finite lifetime of the states involved in the transition together with Heisenberg uncertainty principle results in lifetime broadening with a Lorentzian line-shape function [*Bernath*, 2005]:

$$g(\nu) = \frac{\dfrac{\Delta\nu}{2\pi}}{(\nu - \nu_{nm})^2 + \left(\dfrac{\Delta\nu}{2}\right)^2} \,, \qquad (13)$$

where ν_{nm} is the transition frequency and quantity

$$\Delta\nu = \frac{1}{2\pi}\left(\frac{1}{\tau_n} + \frac{1}{\tau_m}\right), \qquad (14)$$

is proportional to the full width at half maximum (FWHM) of the line. τ_n and τ_m are the lifetimes of the corresponding states. For transitions between bound states at conditions present in plasmatic experiments this type of broadening can be usually neglected. It can be important if the transition involves weakly bound or resonant states or in an ultra-cold regime when other types of broadening disappear [*McGuyer et al.*, 2015].

Collisions of the studied system with other particles give raise to the collisional broadening with Lorentzian line-shape function, where

$$\Delta \nu = \frac{f_{col}}{2\pi}, \tag{15}$$

f_{col} being the collision frequency. The values of pressure broadening are on the order of 10 MHz per 100 Pa [*Bernath*, 2005]. An example of the pressure broadening coefficients measured for the P(6) transition in the (200) ← (000) vibrational band of N_2H^+ in the helium buffer gas [*Shapko et al.*, 2020] are shown in Table I.

Table I. Pressure broadening coefficients B_p obtained by *Shapko et al.* [2020] for the P(6) transition in the (200) ← (000) vibrational band of N_2H^+ in the helium buffer gas.

T (K)	B_P (10^{-21} cm^{-1}cm^3)
78	6.2 ± 0.5
140	7.7 ± 0.6
200	8.9 ± 0.3
300	9.4 ± 0.5

The thermal movement of particles with respect to the radiation source results in Doppler broadening of the absorption line with gaussian line-shape function:

$$g(\nu) = \frac{1}{\sqrt{2\pi}\sigma_D} \exp\left(-\frac{(\nu - \nu_{nm})^2}{2\sigma_D^2}\right), \tag{16}$$

With

$$\sigma_D = \nu_{nm}\sqrt{\frac{k_B T_{kin}}{Mc^2}}, \tag{17}$$

where k_B is the Boltzmann constant, T_{kin} is the kinetic temperature of the measured specie, M is its mass and c is the speed of light.

At 300 K and pressure of several hundred Pa, the Doppler broadening is dominant mechanism for very light ions such as H_3^+. If the mass of the studied ions is higher or the temperature is lower, the collisional broadening cannot be neglected and has

to be taken into account in the data analysis by fitting the data by a Voight profile [*Shapko et al.*, 2020].

Cavity Ring-Down Spectroscopy

Originally developed for measuring the reflectivity of dielectrically coated mirrors [*Herbelin et al.*, 1980; *Anderson et al.*, 1984], Cavity Ring-Down Spectroscopy (CRDS) has been since then utilized in many spectroscopic applications [*O'Keefe et. al.*, 1988; *Berden et al.*, 2009].

In principle, two highly reflective mirrors form stable optical cavity and light trapped in the optical resonator leaks through the mirrors. The resulting signal on the photodetector (ring-down) decays exponentially with time [*Berden et al.*, 2009]:

$$I(v, t) = I(v, 0) \exp\left(-\frac{t}{\tau(v)}\right), \tag{18}$$

where:

$$\tau(v) = \frac{d}{c[A(v) - \ln R(v)]}, \tag{19}$$

d is the distance between the mirrors, *c* is speed of light and *R* is the reflectivity of the mirrors. By measuring the ring-down time constant τ(v) with and without absorbing medium present, one can directly obtain the absolute value of the absorbance *A*. A big advantage of this setup is no need to calibrate the light source for the wavelength dependence of the emitted power.

There are various implementations of the CRDS technique, here only pulsed and continuous wave variants will be discussed.

The reflectivity of the mirrors forming optical cavity of CRDS is very high (*R* ~ 0.999 to 0.9999), therefore the majority of the incoming light is reflected. The transmission of the resonator is also influenced by the interference of the light circulating in the resonator. In the pulsed CRDS technique [*O'Keefe et al.*, 1988] a short high power laser pulse with a duration shorter than the time needed for the photons to transverse the distance between the mirrors is used. The disadvantage of

this method is the necessity to utilize pulsed lasers that have typically broad bandwidth unsuitable for high resolution spectroscopy.

The continuous wave CRDS (cw-CRDS) is a technique developed originally by Romanini [*Romanini et al.*, 1997]. He used continuous wave laser source coupled to the cavity modes of the optical resonator and utilized resonant build-up of intensity to inject enough power through the highly reflective mirrors. The process can be illustrated on ideal Fabry-Perot resonator formed by parallel plane mirrors of infinite dimensions. In such case, the steady state transmission *I* for incident light propagating in a direction perpendicular to the entry mirror is given by [*Yariv*, 1997]:

$$I = I_0 \frac{(1-R)^2}{(1-R)^2 + 4R\sin^2\left(\frac{2\pi d}{\lambda}\right)},$$ (20)

where λ is the wavelength. For some values of d/λ the resonant condition is fulfilled and $I/I_0 = 1$. The corresponding standing waves are called modes of the resonator. Similar result can be obtained for non-planar mirrors, for details see refs. [*Lehmann et al.*, 1996; *Morville*, 2001]. The planar configuration of mirrors is unstable due to finite mirror dimensions [Yariv, 1997] and optical cavity of the CRDS is usually formed by spherical mirrors. In such case the radii of the curvature of the mirrors, r_1 and r_2 have to fulfil equation:

$$0 \leq \left(1 - \frac{d}{r_1}\right)\left(1 - \frac{d}{r_1}\right) \leq 1,$$ (21)

The mode structure of such optical cavity is more complicated than for ideal Fabry-Perot resonator. The solution of Maxwell equations with appropriate boundary conditions involves standing waves with longitudinal modes (analogous to modes in Fabry-Perot resonator, the fundamental mode is denoted TEM$_{00}$) and transverse modes labelled TEM$_{mn}$ with m and n being integers. For details see ref. [*Yariv*, 1997].

To ascertain that the resonant condition for equation (20) is fulfilled, *Romanini et al.* [1997] put one of the mirrors on a piezo element that changed the distance of the mirrors by a value larger than the wavelength of the used light. The resonant

condition is then fulfilled at least twice per cavity sweep. This approach is also utilised in our experimental setup (see in the corresponding section).

Langmuir probe diagnostics

Langmuir Probe, a metal electrode immersed in plasma, is one of the oldest techniques of plasma diagnostics [*Langmuir*, 1923; *Mott-Smith et al.*, 1926]. In principle, the current-voltage characteristic of the probe is utilized to obtain various plasma parameters such as electron number density n_e, electron temperature or distribution function (EEDF). This section will introduce several equations connecting current-voltage characteristic of single cylindrical probe with plasma parameters. If not stated otherwise, it is assumed that following conditions are fulfilled:

1) The probe does not emit electrons
2) Plasma is not disturbed outside a thin layer around the probe
3) The charged particles in plasma consist of singly charged ions and electrons. Negative ions are not present.
4) The velocity distribution of charged particles in plasma is Maxwellian
5) The mean free paths of electrons and ions are substantially longer than the Debye length λ_D.
6) Independence of electron and ion currents.

An example of current voltage characteristic of single probe is plotted in Figure 3. The characteristic can be divided in to three regions depending on the probe voltage U. At plasma potential (U_{pl}, inflexion point of the current-voltage characteristic [*Smith et al.*, 1979]) the probe is neither attractive nor repulsive for charged particles. If $U > U_{pl}$, electrons are attracted to the probe, while the ions are repulsed (saturated electron current region). The electron current i_- collected by the probe is then [*Hutchinson*, 2002]:

18

$$i_- = \sqrt{\frac{2}{m_\mathrm{e}}} \frac{A_\mathrm{probe} e n_\mathrm{e}}{\pi} \sqrt{e U_\mathrm{S} + k_\mathrm{B} T_\mathrm{e}}, \tag{22}$$

where A_probe is the collecting surface of the probe, m_e electron mass, e is the elementary charge, $U_\mathrm{S} = U_\mathrm{p} - U$ and k_B is the Boltzmann constant. The electron density can be obtained from the slope of the dependence of the second power of i_- on U_S (i-square method [*Mott-Smith et al.*, 1926]).

If $U < U_\mathrm{p}$, the probe attracts ions and electrons are repulsed. Some of the electrons have still enough kinetic energy to overcame the repulsive voltage and fall on the probe. The more is the probe negative with respect to the plasma potential, the fewer electrons are collected by the probe resulting in rapid decrease of the measured probe current with decreasing voltage (retarding region). For Maxwellian electron velocity distribution the electron current can be described in this region as [*Pfau et al.*, 2001]:

$$i_- = -e n_\mathrm{e} A_\mathrm{probe} \sqrt{\frac{k_\mathrm{B} T_\mathrm{e}}{2\pi m_\mathrm{e}}} \exp\left(-\frac{e U_\mathrm{S}}{k_\mathrm{B} T_\mathrm{e}}\right). \tag{23}$$

Electron temperature can be determined from the natural logarithm of electron current given by equation (23) or its second derivative. The second derivative of the probe current in the retarding region can be also used to obtain the electron energy distribution function f (EEDF):

$$f(e U_\mathrm{S}) = \frac{2\sqrt{2 m_e U_S}}{n_e e^3 A_{probe}} \frac{\mathrm{d}^2 i_-}{\mathrm{d} U^2}, \tag{24}$$

where f is normalized to unity:

$$\int_0^\infty f(x)\,\mathrm{d}x = 1. \tag{25}$$

Equation (24) derived by Druyvesteyn [*Druyvesteyn*, 1930] is valid also for non-maxwellian EEDF.
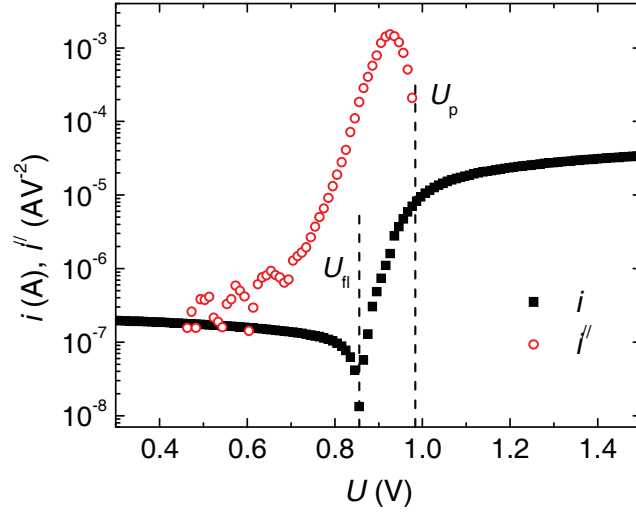
Figure 3. Adapted from ref. [*Dohnal*, 2013]. Absolute value of the current voltage characteristic (full squares) and its second derivative (circles). Positions of floating potential (U_{fl}) and of plasma potential (U_p) are denoted by vertical dashed lines. The characteristic was obtained in Cryo-FALP II experiment in Ar$^+$ dominated helium buffered plasma at $T = 250$ K and $P = 800$ Pa.

The region of the current-voltage characteristic where $U \ll U_p$ is denoted as saturated ion current region. If the electron and ion currents collected by the probe are the same, the overall current is zero and the corresponding voltage is called floating potential U_{fl}.

Microwave diagnostics

The microwaves have been used for plasma parameters determination for over seventy years [*Brown et al.*, 1952; *Larsson et al.*, 2008] and many experimental techniques were developed [*Brown et al.*, 1952; *Torrisi et al.*, 2022]. In some of the presented studies we employed a method based on tracing the changes of the resonance frequency of the cylindrical resonator in dependence on electron number density in the resonator [*Shapko et al.*, 2021]. The shift Δf_r of the resonance frequency f_r is proportional to the electron number density n_e [*Šícha et al.*, 1966]:

$$n_{\mathrm{e}} = \Delta f_{\mathrm{r}} f_{\mathrm{r}} \frac{2\pi m_{\mathrm{e}}}{e_0^2} \frac{\int_V E^2 \mathrm{d}V}{\int_{V'} J_0\left(\frac{2.405}{r_0}\right) E^2 \mathrm{d}V}, \qquad (26)$$

where E is the intensity of the field in the resonator, V and V' are the volume of the resonator and of the plasma column, respectively, J_0 is the Bessel function of the zeroth order, m_{e} and e_0 are the electron mass and charge and r_0 is the radius (inner) of the discharge tube containing the plasma with r being distance from the axis of the resonator.

Experimental techniques

The results presented in this thesis were obtained using two modifications of the stationary afterglow technique (SA-CRDS and Cryo-SA-CRDS) and of the flowing afterglow technique (Cryo-FALP II). A short overview of the experimental setup will be given here.

Cryo-FALP II

Cryogenic Flowing Afterglow with Langmuir Probe is a low temperature modification of the flowing afterglow technique [*Fehsenfeld et al.*, 1966; *Ferguson et al.*, 1969] combined with axially movable Langmuir probe [*Mahdavi et al.*, 1971]. A detailed description of the experimental apparatus can be found e. g. in ref. [*Kotrík*, 2013]. A scheme of the Cryo-FALP II setup is shown in Figure 4.
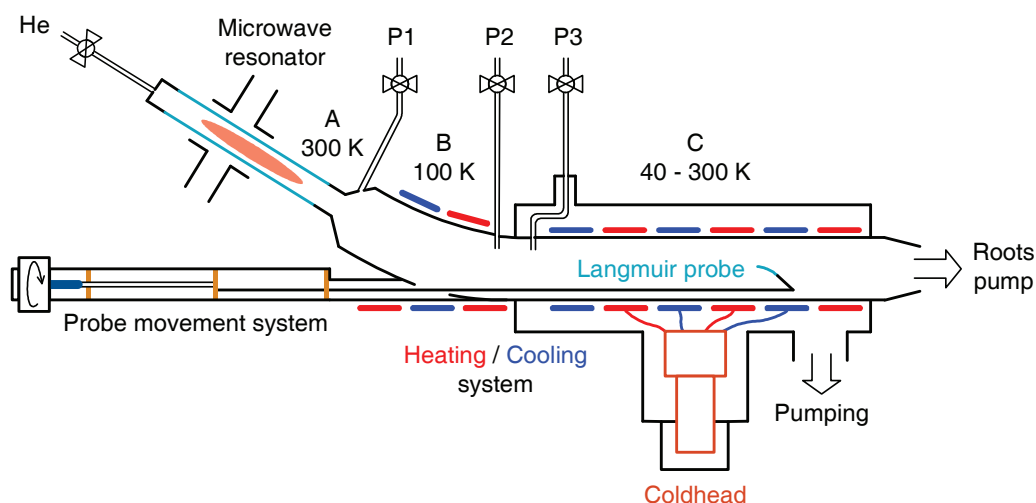
Figure 4. Adapted from ref. [*Kotrik*, 2013]. A scheme of the Cryo-FALP II apparatus.

Helium buffer gas flows through the glass discharge tube where it is ionized by a microwave discharge ignited in a Evenson cavity [*Kotrik*, 2013] and plasma containing electrons, He^+, He_2^+ and helium metastable atoms ($2\,^1S$ and $2\,^3S$ states of helium) is formed. It is then driven to the stainless-steel flow tube with inner

diameter of 5 cm. There are several entry ports for reactants positioned along the flow tube. In this way, the plasma formation and the actual chemistry can be separated as the reactant gases are not subject to the discharge and the reactants can be added at specific position corresponding to the time in the afterglow. The electron number density along the flow tube is probed by a Langmuir probe. At the end of the flow tube, the gas is pumped by a Roots type pump ensuring buffer gas flow on the order of thousands of sccm (~1 – 10 Pa m^3s^{-1}). In some experiments the setup can be modified by addition of a differentially pumped chamber and of a mass spectrometer.

As denoted by capital letters in Figure 4, the flow tube is divided in to three sections with different temperature. Section A, containing discharge tube, is kept at room temperature. Section B is cooled by liquid nitrogen to approximately 100 K. The port at the beginning of this section is usually used to add argon for effective removal of helium metastable atoms. Section C is connected to the cold-head of the closed cycle helium refrigerator enabling measurements in the range of 40 – 300 K. The flow tube itself is positioned inside a vacuum chamber to minimize heat losses. The temperature along the tube is monitored by type T thermocouples and DT-471-CU silicon diodes.

Prior entering the apparatus, the helium buffer gas is purified by passing through molecular sieves kept at liquid nitrogen temperature. Similarly, all the reactant gases are purified using cold traps with liquid nitrogen or precooled ethanol.

The gas handling/mixing system of the apparatus (not shown in Figure 4) enables using reactant number densities as low as 10^{10} cm^3s^{-1}.

Stationary afterglow with Cavity Ring-Down spectrometer

Two modifications of the stationary afterglow setup equipped with Cavity Ring-Down spectrometer were used in presented studies – SA-CRDS and Cryo-SA-CRDS. Both experiments share the gas handling and mixing system with the Cryo-FALP II apparatus.

SA-CRDS is an acronym for Stationary Afterglow apparatus with Cavity Ring-Down Spectrometer. Detailed description can be found e. g. in refs. [*Macko et al.*, 2004; *Dohnal*, 2013] so only short overview will be given here.

The optical system consists of laser source, optical isolator to protect the laser from back reflections, acousto-optic modulator (AOM) for fast switching off the laser beam and spatial filter consisting of two lenses and a pinhole between them. The optical cavity is formed by two mirrors positioned on the optical axis of the apparatus 75 cm apart. The light exiting the cavity is then collected by a detector based on avalanche photodiode and amplifier. The signal is then processed and stored by the data acquisition system.
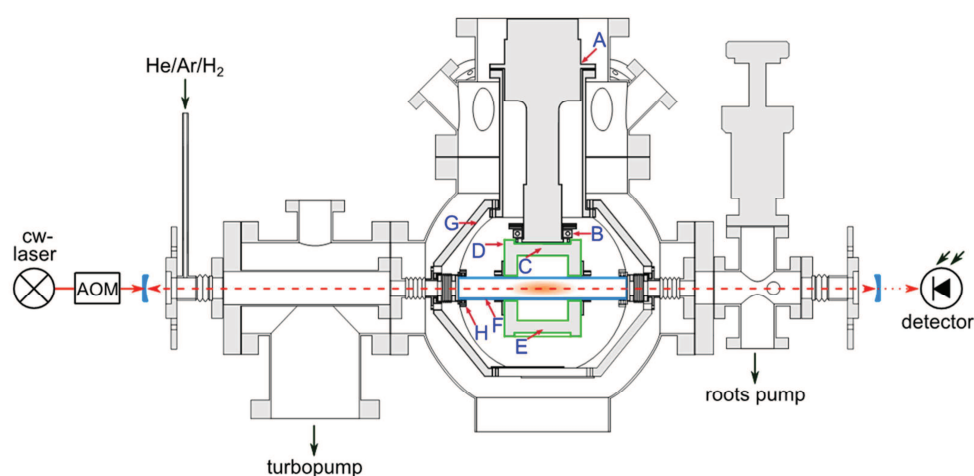
Figure 5. Adapted from ref. [*Shapko et al.*, 2021]. A scheme of the Cryo-SA-CRDS apparatus.

The fused silica discharge tube of the SA-CRDS apparatus is placed inside a microwave resonator cavity enabling discharge ignition. The tube is cooled by liquid nitrogen or liquid nitrogen vapours enabling operation in the temperature range 80 – 300 K. In some experiments, heating elements were placed at both ends of the discharge tube, outside of the microwave resonator, to heat up the tube to approximately 350 K [*Shapko et al.*, 2020].

During the experiments, discharge is periodically ignited in a mixture of gases and then switched off after set time. The time evolution of the ion number density in discharge and afterglow plasma is then probed by cavity ring-down spectrometer.

24

The Cryogenic Stationary Afterglow apparatus with Cavity Ring-Down Spectrometer (Cryo-SA-CRDS) is a low temperature modification of the SA-CRDS setup [*Plašil et al.*, 2018]. A scheme of the apparatus is shown in Figure 5. It shares many properties of the SA-CRDS setup (gas handling system, similar optical setup) but there are important alterations highly enhancing its capabilities.

The cold head of the closed cycle helium refrigerator is connected to the microwave resonator (green in Figure 5) and it is in turn attached by copper braids to the discharge tube made of monocrystalline sapphire. This enables to prepare ions with kinetic temperatures (evaluated from the Doppler broadening of the absorption lines) as low as 30 K [*Plašil et al.*, 2018]. The discharge tube and cold-head are inside a vacuum chamber to ensure thermal insulation.

As the microwave resonator has no movable parts, to ensure the effective coupling of the microwaves to the resonator, it is necessary to tune the frequency of the microwaves to the resonant frequency of the microwave resonator. I have designed a microwave source based on solid state microwave synthetiser (SLSM5 from Luff Research Inc) that can produce microwaves in the range of 2.4 – 2.6 GHz. The low power (~ 10 mW) microwave radiation can then be switched on and off very fast (rise and fall time of less than 1 μs) by a PIN switch. The microwave signal is then amplified by an amplifier to 10 – 20 W that is enough to ignite the discharge.

In addition to the cavity ring-down spectroscopy, Cryo-SA-CRDS apparatus is equipped by microwave diagnostics, based on tracing the shift of the resonant frequency of the microwave cavity, for electron number density determination. As a source of probing microwaves, I used the same setup as for plasma ignition but without the amplifier stage. In connection with the data acquisition system, this enables measurements of the evolution of the electron number density in afterglow plasma with an effective time resolution of 2.5 μs. The detailed description of the setup can be found in ref. [*Shapko et al.*, 2021].

The ability of the Cryo-SA-CRDS apparatus to probe at the same time electron number density and the number density of the ions of interest is crucial for reliable recombination rate coefficient determination even at conditions when the studied ions are not dominant ionic species in the afterglow [*Shapko et al.*, 2021].

Data analysis

In quasineutral afterglow plasma containing singly charged ionic specie A^+ the time evolution of the electron number density can be described by differential equation:

$$\frac{dn_A}{dt} = -\alpha\, n_A n_e - \frac{n_A}{\tau}, \tag{27}$$

where n_A and n_e are number densities of ions A^+ and of electrons, α is the recombination rate coefficient and τ denotes the losses of ions by ambipolar diffusion and by reactions (ion-molecule reaction, three-body association reaction, etc.):

$$\frac{1}{\tau} = \frac{1}{\tau_D} + \frac{1}{\tau_R}, \tag{28}$$

here τ_D stands for ambipolar diffusion losses (assuming only fundamental diffusion mode) and τ_R denotes reaction losses.

If A^+ is dominant ionic specie in afterglow plasma, then $n_A = n_e$ and equation (27) has an analytical solution:

$$n_e(t) = \frac{1}{\alpha\tau\left(\exp\left(\frac{t-t_0}{\tau}\right) - 1\right) + \frac{1}{n_0}\exp\left(\frac{t-t_0}{\tau}\right)}, \tag{29}$$

that can be used to determine the recombination rate coefficient by directly fitting the data. Here n_0 is the electron number density at time $t = t_0$.

If A^+ is not dominant ionic specie at the beginning of the afterglow but gradually becomes dominant a technique called "Integral analysis" can be employed [*Korolov et al.*, 2008]. Let's define the fraction of ions A^+ with respect to all ions as $\xi(t) = n_A(t)/n_e(t)$. Fraction $\xi(t)$ varies with time and becomes unity when A^+ is a dominant ion in the afterglow. The time evolution of the electron number density in afterglow can then be rewritten as:

$$\frac{dn_e}{dt} = -\alpha\xi(t)n_e^2 - \frac{n_e}{\tau}, \tag{30}$$

which after integration gives:

$$\ln\left[\frac{n_e(t_b)}{n_e(t_a)}\right] + \frac{(t_b - t_a)}{\tau} = -\alpha \int_{t_a}^{t_a} \xi(t)n_e dt, \qquad (31)$$

Where t_a and t_b are integration limits. When the studied ion becomes dominant, $\xi(t) = 1$ and the plot of the left-hand side of equation (31) in dependence on the integral on the right-hand side gives a straight line with a slope $-\alpha$. In this procedure, τ is a variable parameter determined by minimizing the χ^2 of a given fit.

If the plasma deionisation is dominated by recombination assisted by collisions with electrons as third particles (as in the case of $Ar^+ + e^- + e^- \rightarrow Ar + e^-$ recombination studied in ref. [*Dohnal et al.*, 2013]), α in equation (30) depends on n_e:

$$\alpha = K_{E-CRR}n_e, \qquad (32)$$

where K_{E-CRR} is the ternary coefficient for electron assisted collisional radiative recombination and for $\xi = 1$ is the analytical solution of equation (30):

$$\iota_e(t) = \frac{1}{\left(\alpha\tau\left(\exp\left(2\frac{t-t_0}{\tau}\right) - 1\right) + \frac{1}{n_0^2}\exp\left(2\frac{t-t_0}{\tau}\right)\right)^{1/2}}, \qquad (33)$$

while the "Integral analysis" has the form [*Dohnal et al.*, 2013]:

$$\ln\left[\frac{n_e(t_b)}{n_e(t_a)}\right] + \frac{(t_b - t_a)}{\tau} = -K_{E-CRR}\int_{t_a}^{t_a} \xi(t)n_e^2 dt. \qquad (34)$$

Let's assume a more general case when ions A^+ are not necessarily dominant in the afterglow but they are no longer formed. In SA-CRDS or Cryo-FALP II experiment based either on ion or on electron number density determination the mentioned data analysis techniques would lead to erroneous results. The Cryo-SA-CRDS apparatus enables simultaneous determination of the time evolutions of both electron and ion number densities so all the time dependent quantities in equation (27) are known and it can be solved by direct integration [*Shapko et al.*, 2021]:

$$n_A(t_i) = n_A(t_0)e^{-\alpha X(t_i) - \frac{1}{\tau}Y(t_i)}, \qquad (35)$$

where

$$X(t_{\mathrm{i}}) = \int_{t_0}^{t_{\mathrm{i}}} n_{\mathrm{e}}(t)\mathrm{d}t, \tag{36}$$

and

$$Y(t_{\mathrm{i}}) = t_{\mathrm{i}} - t_0. \tag{37}$$

Note that n_{A}, $X(t_{\mathrm{i}})$ and $Y(t_{\mathrm{i}})$ are measured in Cryo-SA-CRDS experiment (or can be calculated from measured quantities), so we can find the parameters $n_{\mathrm{A}}(t_0)$, α and τ that fulfil the equation (35) in the least square sense.
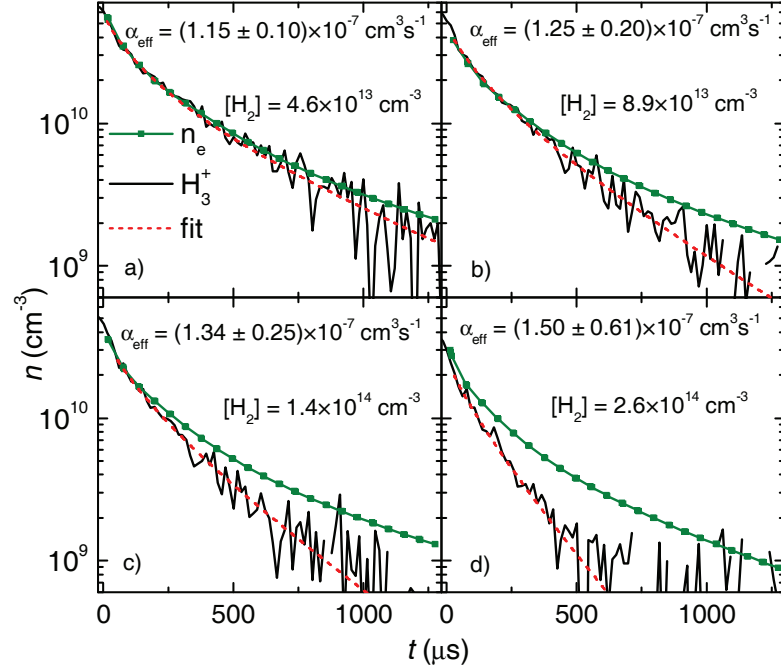
Figure 6. Adapted from ref. [*Shapko et al.*, 2021]. The time evolutions of electron (squares) and H_3^+ (full line) number densities obtained in Cryo-SA-CRDS experiment in helium buffered afterglow plasma at different number densities of H_2. The dashed line is a fit to the data by equation (35). The corresponding effective recombination rate coefficients are written in each panel, the displayed error being the statistical error of the fit. The conditions of the experiments were: $T = 200$ K, $[He] = 3\times10^{17}$ cm^{-3}, $[Ar] = 2\times10^{14}$ cm^{-3} and $[H_2]$ in the range of 4.6×10^{13} to 2.6×10^{14} cm^{-3}.

Examples of the time evolutions of H_3^+ and electron number densities measured in the Cryo-SA-CRDS experiment are plotted in Figure 6. In panel a) of Figure 6 the H_3^+ ions are dominant ions in the afterglow plasma. As the number density of H_2 increases, H_5^+ ions are formed in the three-body association reaction of H_3^+ with H_2 and helium. In panel d) the H_3^+ ions are no longer dominant in later afterglow but the recombination rate coefficient evaluated by fitting the data by equation (35) is within the error of the measurement the same as in panel a) of Figure 6.

We also tested the data analysis procedure on a case of H_3^+ ions in neon buffer gas. Here, due to unfavourable chemistry, the fraction of H_3^+ ions in the afterglow was less than one half of all ions the rest being mainly NeH^+ (the formation of H_3^+ from the reaction of NeH^+ with H_2 is very slow). Nevertheless, the evaluated effective recombination rate coefficient for H_3^+ ions was within error of the measurement the same as for H_3^+ ions in helium gas of the same number density. For details see ref. [*Shapko et al.*, 2021].

As a side note, as the left and right-hand side of equation (27) depends on the same order of n_A, the result of the fitting by equation (35) is largely insensitive to systematic errors in n_A determination (e. g. uncertainty in transition line strength or the length of absorbing medium).

Results

Recombination of H_3^+ with electrons – third-body assisted recombination and the effect of nuclear spin

H_3^+, the simplest polyatomic ion and the most abundantly produced molecular ion in interstellar medium [*Oka*, 2006] is considered to play a key role in reaction chains leading to formation of complex molecules in interstellar space [*Oka*, 2006; *Millar*, 2015]. In fact, the importance of H_3^+ ions for interstellar chemistry was established [*Herbst et al.*, 1973] long before its actual detection [*Geballe et al.*, 1996].

The dissociative recombination is the main destruction process for H_3^+ ions in interstellar medium [*Larsson et al.*, 2008] and as such has been studied for over 70 years. The actual value of the recombination rate coefficient has been subject of controversies with the results of various experimental groups differing by orders of magnitude. Table II summarizes values of the recombination rate coefficient for recombination of H_3^+ ions with electrons obtained starting in the late forties.

Some of the inconsistencies in afterglow experiments were resolved by discovery of surprisingly fast third-body assisted recombination of H_3^+ ion in helium buffer gas by Glosik and co-workers [*Glosík et al.*, 2008] who showed that when the H_3^+ recombination rate coefficients are plotted with respect to helium number density, they can be fitted by a straight line: $\alpha_{eff} = \alpha_{bin} + K_{He}[He]$. The inferred binary recombination rate coefficient α_{bin} was then in a good agreement with the results of the latest ion storage ring study performed with vibrationally cold ions [*McCall et al.*, 2004]. A third-body assisted recombination process of magnitude similar to that of H_3^+ was later observed for its deuterated isotopologues [*Kotrík et al.*, 2010; *Dohnal et al.*, 2012c; *Dohnal et al.*, 2016; *Plašil et al.*, 2017]. When the helium buffer gas is exchanged for neon, the measured H_3^+ recombination rate coefficients are within the error of the measurement the same as in ambient helium [*Shapko et al.*, 2021] while we observed a substantially larger ternary recombination rate coefficient for hydrogen buffer gas [*Dohnal et al.*, 2014; *Glosík et al.*, 2015]. The ternary recombination rate coefficients K_{He} and K_{H2} for H_3^+ ions obtained in our various studies are plotted in Figure 7.

Table II. Recombination rate coefficient as measured for H_3^+ ions in different experiments using normal H_2 (ortho to para nuclear spin state ratio of 3:1). Adapted from refs. [*Plašil et al.*, 2002; *Dohnal* 2013]. SA − stationary afterglow, μw − microwave diagnostics, IB − inclined beam, MB − merged electron-ion beam, IT − ion trap, FALP − flowing afterglow with Langmuir probe, IR − infrared spectroscopy in stationary afterglow setup, SR − ion storage ring, C1, C2 − compilations of multiple experiments.

Year	α (10^{-7} cm^{3}s^{-1})	Method	Comment	Reference
1949	25	SA/μw		[*Biondi et al.*, 1949b]
1951	20 and 60	SA/μw	1 and 7 torr, H_2	[*Richardson et al.*, 1951]
1951	3 and 25	SA/μw	3 and 30 torr, H_2	[*Varnerin et al.*, 1951]
1955	<0.3	SA/μw		[*Persson et al.*, 1955]
1973	2.3	SA/μw	300 K	[*Leu et al.*, 1973]
1974	2.5	IB		[*Peart et al.*, 1974]
1977	2.1	MB		[*Auerbach et al.*, 1977]
1978	1.5	IT		[*Mathur et al.*, 1978]
1979	2.1	MB		[*McGowan et al.*, 1979]
1984	<0.2	FALP		[*Adams et al.*, 1984]
1984	1.5	SA		[*MacDonald et al.*, 1984]
1988	0.2	MB		[*Hus et al.*, 1988]
1989	<0.0001	FALP	Estimate	[*Adams et al.*, 1989]
1990	1.8	IR	273 K	[*Amano*, 1990]
1992	1.5	FALP-MS	300 K	[*Canosa et al.*, 1992]
1993	0.1-0.2	FALP		[*Smith et al.*, 1993]
1994	<2	IR		[*Feher et al.*, 1994]

Table II. Continued from previous page.

Year	α (10^{-7} cm^{3}s^{-1})	Method	Comment	Reference
1994	1.15	SR	CRYRING	[*Sundstrom et al.*, 1994]
1995	1.4-2	FALP		[*Gougousi et al.*, 1995]
1998	0.78	FALP-MS		[*Laubé et al.*, 1998]
1999	0.7	SR	TARN II	[*Tanabe et al.*, 1999]
2000	<0.13	SA	[H$_2$] < 10^{11} cm^{-3}	[*Glosík et al.*, 2000]
2001	1	SR	ASTRID	[*Jensen et al.*, 2001]
2003	1.7	FALP	250 K	[*Glosík et al.*, 2003]
2004	0.68	SR	CRYRING	[*McCall et al.*, 2004]
2004	1.6	IR	330 K	[*Macko et al.*, 2004]
2008	0.75	FALP, C1	260 K	[*Glosík et al.*, 2008]
2013	0.6	FALP, C2	300 K	[*Rubovič et al.*, 2013]
2015	0.6	FALP, IR	300 K	[*Hejduk et al.*, 2015]

Some of the values of the recombination rate coefficients obtained in afterglow experiments are very low and cannot be explained by third-body assisted recombination (see refs. [*Adams et al.*, 1984; *Adams et al.*, 1989; *Smith et al.*, 1993; *Glosík et al.*, 2000]). Smith et al. [*Smith et al.*, 1993] in fact observed a fast decay of electron number density in early afterglow and argued that vibrationally excited H_3^+ ions are responsible and $H_3^+(v = 0)$ recombination is a slow process. Glosík et al. [*Glosík et al.*, 2000] reported a very low value of the recombination rate coefficient for low number densities of reactant hydrogen while for [H$_2$] > 10^{12} cm^{-3} the value of the recombination rate coefficient saturates at $\alpha_{eff} \approx 10^{-7}$ cm^{3}s^{-1}. Note that at low H$_2$ number densities the H_3^+ ions have on average less than one collision with hydrogen prior recombination so their internal states populations could have been far from equilibrium.
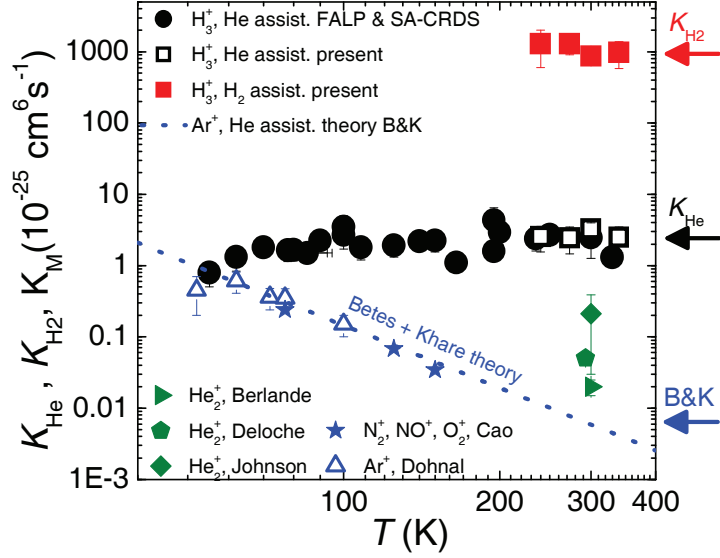
Figure 7. Adapted from ref. [*Glosík et al.*, 2015]. The dependence of the values of ternary recombination rate coefficients on temperature for helium (open squares and full circles [*Glosík et al.*, 2009; *Varju et al.*, 2011; *Dohnal et al.*, 2012a; *Johnsen et al.*, 2013]) and hydrogen (full squares [*Glosík et al.*, 2015]) buffer gas. The values of K_{He} obtained by us for Ar^+ ions [*Dohnal et al.*, 2013] and by other groups for He_2^+ [*Berlande et al.*, 1970; *Johnson* 1971; *Deloche et al.*, 1976] and a mixture of atmospheric ions in helium [*Cao et al.*, 1991] are plotted for comparison. Theoretical value scaled for Ar^+ ions in helium [*Bates et al.*, 1965] is plotted as dotted line.

In the last ten years I and my co-workers used improvements in instrumentation to characterize the H_3^+ dominated afterglow plasma used for recombination rate coefficient determination. We have shown that at conditions under which the values of the H_3^+ recombination rate coefficient were reported in refs. [*Glosík et al.*, 2008; *Rubovič et al.*, 2013; *Hejduk et al.*, 2015], the rotational and nuclear spin state populations of the recombining ions are in accordance with thermal equilibrium at given temperature, the electron temperature is close to the temperature of the buffer gas (with a rather large systematic error of $40 - 70$ K [*Dohnal et al.*, 2013; *Hejduk et al.*, 2015; *Kálosi et al.*, 2016]) and that the H_3^+ ions are dominant ions in the afterglow and predominantly in their ground vibrational state (see panel a) of Figure 6 and ref. [*Shapko et al.*, 2021]). The same can be stated for our studies focused on determination of the nuclear spin state selective recombination rate coefficients for

33

H_3^+ ions that will be described below, with an exception of the nuclear spin state populations that are given by the nuclear spin state population of the used hydrogen gas.

For a long time, the theoretical predictions suggested that the recombination of H_3^+ ions with electrons will be very slow at low collisional energies due to lack of favourable potential curve crossings. The inclusion of the Jahn-Teller mechanism into the calculations [*Kokoouline et al.*, 2001] led to the increase of the calculated recombination rate coefficient by orders of magnitude and after some refinement [*Fonseca dos Santos et al.*, 2007; *Pagani et al.*, 2009; *Jungen et al.*, 2009] to a very good agreement with afterglow and ion storage ring data at 300 K.

The most recent theory [*Pagani et al.*, 2009] predicts that at low, astrophysically relevant, temperatures the recombination rate coefficients for ortho and para nuclear spin states of H_3^+ differ by a factor of four or more. The groups based around TSR and CRYRING ion storage rings confirmed that para-H_3^+ ions recombine faster than ortho-H_3^+ but only small enhancement was observed at low collisional energies [*Tom et al.*, 2009; *Kreckel et al.*, 2010]. Note that the rotational temperature of the H_3^+ ions in the ion storage ring experiment was probably 300 K or higher [*Petrignani et al.*, 2011].

We have studied the recombination of ortho- and para-H_3^+ ions utilizing the ability of our SA-CRDS experimental setup to probe in situ the time evolutions of different quantum states of H_3^+ ions. The recombination rate coefficient was first measured using normal hydrogen (thermal nuclear spin state ortho to para ratio of 3:1 at 300 K) and then the measurement was repeated using the same experimental conditions but with H_2 gas passing through paramagnetic catalyst leading to ortho to para ratio of 90:10 or better [*Zymak et al.*, 2013]. In this way we were able to obtain the nuclear spin state specific recombination rate coefficients for H_3^+ ions in the temperature range of $80 - 300$ K [*Varju et al.*, 2011; *Dohnal et al.*, 2012a; *Dohnal et al.*, 2012b]. Later, we used the ortho-H_3^+ and para-H_3^+ populations determined in SA-CRDS to extend these measurements to 60 K using the Cryo-FALP II setup where the direct determination of nuclear spin state populations of recombining ions is not possible [*Hejduk et al.*, 2015].
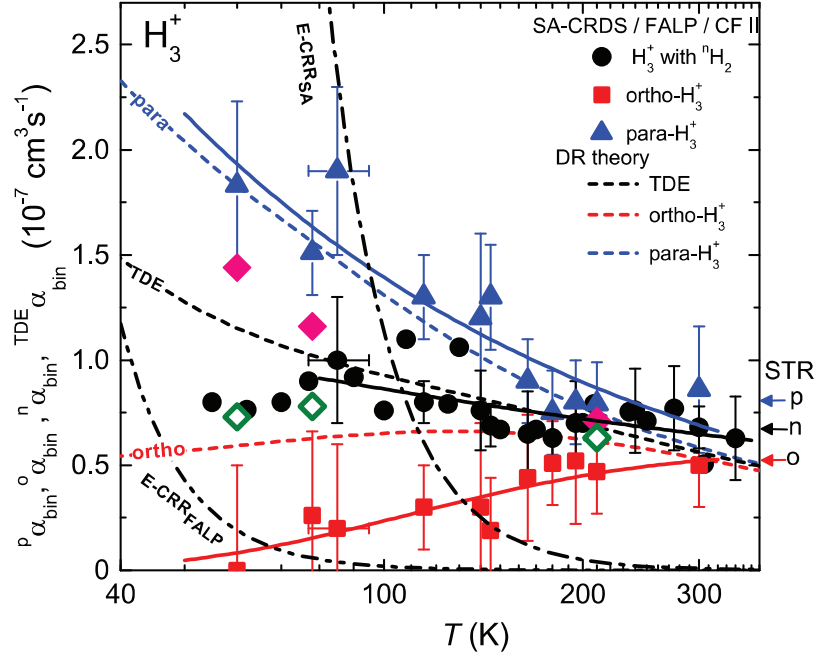
Figure 8. Adapted from ref. [*Hejduk et al.*, 2015]. A compilation of nuclear spin state specific binary recombination rate coefficients obtained in Cryo-FALP II [*Hejduk et al.*, 2015] and SA-CRDS experiments [*Varju et al.*, 2011; *Dohnal et al.*, 2012a]. The values for para-H_3^+ and ortho-H_3^+ ions are plotted as triangles and squares, respectively. The open and full diamonds denote values of binary recombination rate coefficient measured in Cryo-FALP II experiment in normal or para enriched hydrogen gas, respectively, while the full circles are values of binary recombination rate coefficient for H_3^+ ions obtained using normal hydrogen in our previous studies [*Dohnal et al.*, 2012a; *Rubovič et al.*, 2013]. Full lines are fits to the corresponding recombination rate coefficients (for details see ref. [*Hejduk et al.*, 2015]). The dashed lines labelled "ortho", "para" and "TDE" denote theoretical predictions by Pagani et al. [*Pagani et al.*, 2009] for ortho-H_3^+, para-H_3^+ and H_3^+ ions with thermal populations of states, respectively. The arrows on the right-hand side of the figure denote values of the corresponding recombination rate coefficients measured at 300 K in ion storage ring experiment CRYRING [*Tom et al.*, 2009].

The binary recombination rate coefficients obtained for ortho-H_3^+, para-H_3^+ and H_3^+ with thermal population of nuclear spin states are shown in Figure 8. As can be seen from the figure, at 300 K the recombination rate coefficients for ortho-H_3^+ and para-

H_3^+ are the same within the error of the measurement and very close to the values reported in CRYRING experiment for 300 K [*Tom et al.*, 2009]. As the temperature decreases the difference between the measured recombination rate coefficients for ortho and para nuclear spin states of H_3^+ increases in excellent confirmation of theoretical predictions [*Pagani et al.*, 2009].

It is necessary to note that the models of diffuse interstellar gas clouds are unable to get agreement with astronomical observations when our or theoretical recombination rate coefficients for ortho- and para-H_3^+ ions are used [*Albertsson et al.*, 2014]. The best fit between calculations and observations was achieved when ortho- and para-H_3^+ ions recombined with the same recombination rate coefficient with a value two times higher than that reported in CRYRING experiment [*McCall et al.*, 2004]. Some piece of the puzzle is evidently missing – the production (cosmic rate ionisation), the destruction (dissociative recombination) or the nuclear spin state specific reactions between ortho/para-H_3^+ and ortho/para-H_2. Clearly more experimental work is needed to solve this conundrum. I hope that the new ion storage ring in Heidelberg [*von Hahn et al.*, 2016] will address this issue.

In order to extend our recombination studies to lower temperatures, we developed the Cryo-SA-CRDS apparatus enabling operation in the temperature range of 30 – 300 K. A detailed description of this apparatus can be found in corresponding section of this thesis or in ref. [*Plašil et al.*, 2018].

One of the first tests of the new experimental setup was preparation of cold H_3^+ ions with kinetic temperature around 30 K. At such temperature, almost all H_3^+ ions are in the lowest ortho state (1,0) or in the lowest para state (1,1) of H_3^+. Changing the nuclear spin populations of H_3^+ using procedure described above then results in different population of these two rotational states of H_3^+ [*Dohnal et al.*, 2019]. An example of absorption line profiles obtained with normal H_2 (ortho to para ratio of 3:1) and almost pure para hydrogen gas is shown in Figure 9. Thus, we can change the population of the lowest rotational state (1,1) from 46 % up to 83 % of all H_3^+ ions, the remainder being mainly in the (1,0) state. This opens way to recombination study focused on reactivity of particular low-lying rotational states of H_3^+.
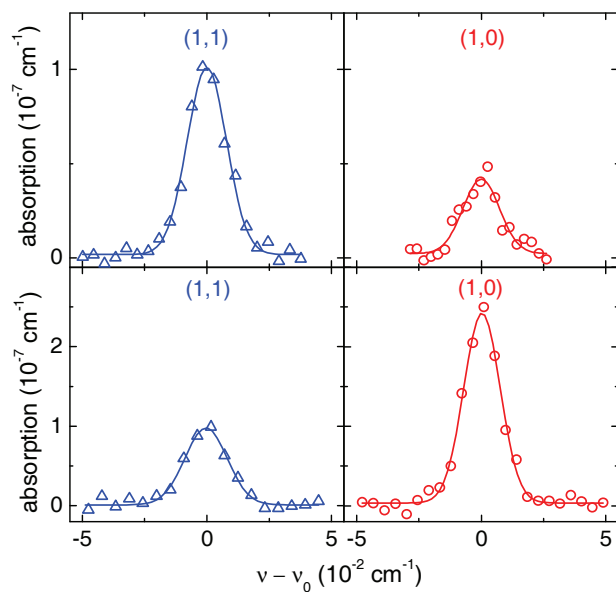
Figure 9. Adapted from ref. [*Dohnal et al.*, 2019]. The absorption line profiles obtained in Cryo-SA-CRDS experiment at 35 K for the two lowest rotational states of H_3^+: ortho-H_3^+(1,0) and para-H_3^+(1,1). Upper panels: fraction of para-H_2 in used hydrogen gas was $^p f_2 = 0.995 \pm 0.005$. Lower panels: the same as in upper panels, $^p f_2 = 0.25$.

Recombination of H_2D^+ and HD_2^+ with electrons

The deuterated isotopologues of H_3^+ – H_2D^+, HD_2^+ and D_3^+ – are produced in interstellar medium in a reaction chain starting with collision of H_3^+ with HD molecule [*Hugo et al.*, 2009]. H_2D^+ and HD_2^+ were detected in interstellar medium [*Tennyson et al.*, 2001; *Millar*, 2005; *Parise et al.*, 2011] and all four isotopologues play an important part in present chemical models of interstellar molecular clouds [*Albertsson et al.*, 2013; *Sipila et al.*, 2013; *Das et al.*, 2015]. The dissociative recombination with electrons is an important loss process for these ions in interstellar medium and one of the pathways for production of D atoms [*Roberts et al.*, 2004; *Sipila et al.*, 2013].

Theoretical calculations by Pagani et al. [*Pagani et al.*, 2009] suggest that H_2D^+ should recombine with electrons faster than HD_2^+ by a factor of three at low temperatures prevalent in molecular gas clouds while only small isotopic effect is predicted by Jungen et al. [*Jungen et al.*, 2009].

In contrast to the breadth of experimental data focused on H_3^+ recombination with electrons there are only few studies concerning H_2D^+ and HD_2^+. The recombination cross sections for HD_2^+ ions were measured in merged-beam experiment by Mitchell et al. [*Mitchell et al.*, 1984] and the cross sections and recombination rate coefficients for H_2D^+ and HD_2^+ ions were also obtained by ion storage ring CRYRING [*Datz et al.*, 1995; *Zhaunerchyk et al.*, 2008], while the relative cross sections and product branching ratios were measured in ion storage ring TSR [*Lammich et al.*, 2003; *Strasser et al.*, 2004].

Unfortunately, the rotational populations of the ions in ion storage ring experiments were probably pertaining to the temperature of 300 K [*Petrignani et al.*, 2011] so the applicability of these results for cold interstellar medium is questionable.

Until 2016, there were no studies of dissociative recombination of H_2D^+ and HD_2^+ in plasma afterglows. This is not surprising as it is extremely difficult to prepare afterglow plasma with either H_2D^+ or HD_2^+ as dominant ions. An example of the dependence of the fractional populations of H_3^+ and its deuterated isotopologues on

the relative fraction of deuterium in hydrogen/deuterium mixture used in a stationary afterglow experiment SA-CRDS is shown in Figure 10.

As can be seen from Figure 10 we were unable to produce plasma with fractional populations of H_2D^+ or HD_2^+ substantially higher than 0.3. A similar behaviour was observed also at 80 K and 125 K. To surmount these obstacles, I decided to utilize the properties of the SA-CRDS setup – the ability to probe in situ number densities of particular ionic states. Light from several DFB (distributed feedback) laser diodes and an external cavity diode laser covering overtone transitions of H_3^+, H_2D^+, HD_2^+ and D_3^+ was directed on the same optical path and then coupled in to the optical cavity of the SA-CRDS apparatus. In this way, we were able to probe the time evolutions of number densities of all isotopomers of H_3^+ in discharge and afterglow plasma.
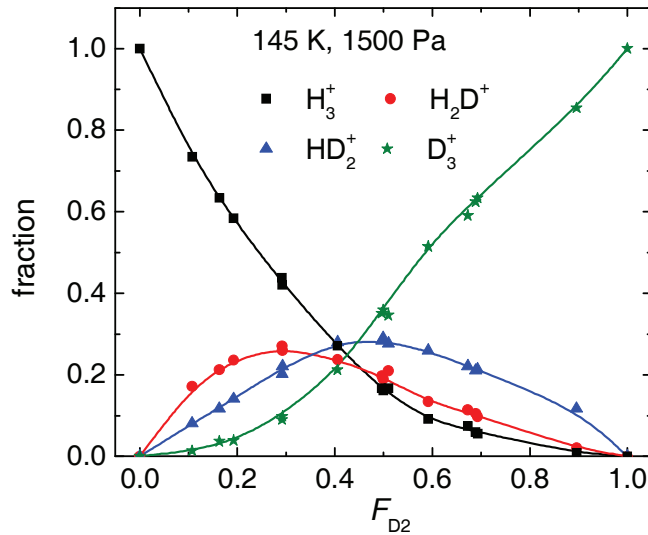
Figure 10. Adapted from ref. [*Plašil et al.*, 2017]. The dependences of the fractional populations of H_3^+, H_2D^+, HD_2^+ and D_3^+ on F_{D2} = [D_2]/([H_2] + [D_2]) obtained in SA-CRDS experiment at 145 K with helium buffer gas pressure of 1500 Pa and [H_2] + [D_2] = 1×10^{14} cm^{-3}. The full lines are for eye guiding only. The data were obtained using known absorption lines of particular ions. For details see in refs. [*Dohnal et al.*, 2016; *Plašil et al.*, 2017].

Assuming plasma quasineutrality and that the H_3^+ isotopomers are dominant ionic species in the afterglow, the measured effective recombination rate coefficient can be written as:

$$\alpha_{\text{eff}} = \alpha_{\text{H3+}}f_{\text{H3+}} + \alpha_{\text{H2D+}}f_{\text{H2D+}} + \alpha_{\text{HD2+}}f_{\text{HD2+}} + \alpha_{\text{D3+}}f_{\text{HD3+}}, \qquad (38)$$

where α_i and f_i are the recombination rate coefficient and the relative fraction of respective isotopomer. Fortunately, f_i did not significantly change in the afterglow plasma and were considered constant in the data analysis. Similarly to H_3^+ and D_3^+ recombination, the $\alpha_{\text{H2D+}}$ and $\alpha_{\text{HD2+}}$ depended on buffer gas pressure due to helium assisted three-body recombination. At given temperature and buffer gas pressure we measured the dependence of the effective recombination rate coefficient (obtained from the time evolution of the sum of number densities of all isotopomers) on $F_{\text{D2}} = [D_2]/([H_2] + [D_2])$. We utilized the binary and ternary recombination rate coefficients for H_3^+ and D_3^+ measured in our previous studies using the same or similar experimental setup [*Dohnal et al.*, 2012a; *Dohnal et al.*, 2012b; *Dohnal et al.*, 2012c; *Hejduk et al.*, 2015] and the probed fractions f_i to evaluate binary and ternary recombination rate coefficients for H_2D^+ and HD_2^+. The binary recombination rate coefficients obtained at three different temperatures are plotted in Figure 11.

As can be seen from Figure 11, the error of the obtained binary recombination rate coefficients is quite high but the disagreement with theoretical calculations by Pagani et al. [*Pagani et al.*, 2009] for H_2D^+ ions is evident, especially at low temperatures. It is important to note, that these values are the only low temperature recombination rate coefficients available for H_2D+ and HD_2^+ ions, where the rotational populations of recombining ions were measured in situ. I am looking forward to the new generation of ion storage rings (for example CSR in Heidelberg [*von Hahn et al.*, 2016]) to bring forth rotationally resolved recombination rate coefficients and confirm (or refute) our results.
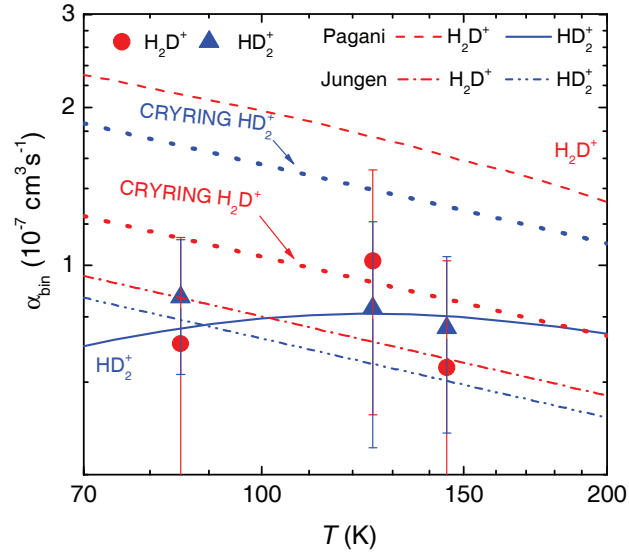
Figure 11. Adapted from ref. [*Plašil et al.*, 2017]. Temperature dependence of the binary recombination rate coefficients for H_2D^+ and HD_2^+ ions. Quantum mechanical calculations by Jungen and Pratt [*Jungen et al.*, 2009; *Pratt et al.*, 2011] (H_2D^+ - dot-dashed line, HD_2^+ – double-dot-dashed line) and by Pagani et al. [*Pagani et al.*, 2009;] (H_2D^+ – dashed line, HD_2^+ – full line) are plotted for comparison. Dotted lines denoted by label "CRYRING" show the values obtained in ion storage ring experiment CRYRING [*Datz et al.*, 1995; *Zhaunerchyk et al.*, 2008] at 300 K and extrapolated to lower temperatures by using $T^{-0.5}$ dependence.

The measured recombination rate coefficients were dependent on helium buffer gas number density with the corresponding values of ternary recombination rate coefficients on the order of 10^{-25} cm^{6}s^{-1} i.e. similar to those observed for H_3^+ and D_3^+ ions. For more details on the H_2D^+ and HD_2^+ recombination experiments see refs. [*Dohnal et al., 2016*; *Plašil et al.*, 2017].

Recombination of D_3^+ with electrons

Although part of models of interstellar chemistry, and so far, not yet observed in interstellar medium, the recombination of D_3^+ with electrons has not enjoyed such spotlight as that of H_3^+. Nevertheless, there are several afterglow [*Smith et al.*, 1993; *Laube et al.*, 1998; *Poterya et al.*, 2002; *Novotny et al.*, 2006], merged electron – ion beam [*van der Donk et al.*, 1991] and ion storage ring [*Larsson et al.*, 1997; *Le Padellec et al.*, 1998] studies focused on this ion mainly by groups that also studied the dissociative recombination of H_3^+ with electrons.

For a long time, the theoretical predictions insisted that D_3^+ ions will recombine only very slowly with electrons [*Larsson et al.*, 2008]. Mirroring the theoretical advances in H_3^+ recombination, the inclusion of Jahn-Teller coupling mechanism led to substantial increase of the calculated recombination rate coefficients [*Pagani et al.*, 2009; *Pratt et al.*, 2011] and to good agreement with the most recent afterglow [*Dohnal et al.*, 2012c] and ion storage ring [*Le Padellec et al.*, 1998] data.

Unsurprisingly, the same disagreements between data obtained by different groups as was observed for H_3^+ recombination take place also for its fully deuterated isotopologue. In case of H_3^+ ions, some of these disagreements were resolved when Glosik et al. [*Glosik et al.*, 2008] discovered surprisingly fast helium assisted three body recombination process for H_3^+ ions. Me and my co-workers then focused on D_3^+ recombination using cryogenic modification of FALP technique (Cryo-FALP II) and stationary afterglow with cavity ring-down spectrometer (SA-CRDS).
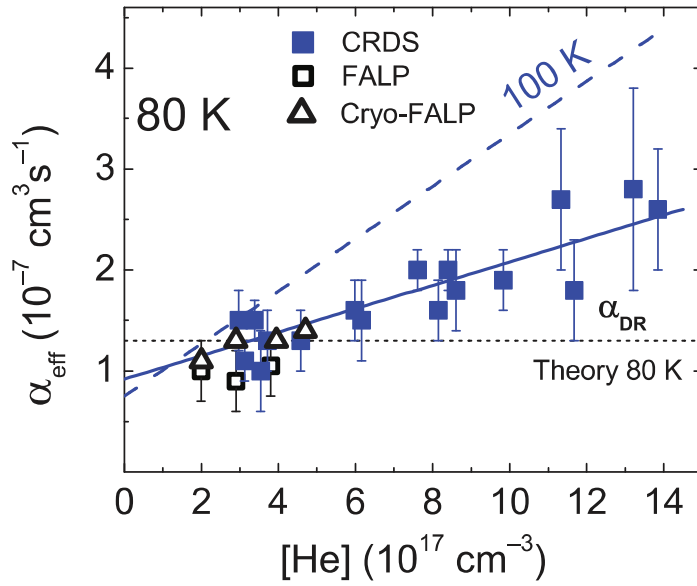
Figure 12 . Adapted from ref. [*Dohnal et al.*, 2012c]. Dependence of the effective recombination rate coefficient for D_3^+ ions on helium number density at 80 K. The data were obtained in the SA-CRDS experiment (full squares) [*Dohnal et al.*, 2012c] and using various modifications of the FALP technique (triangles and open squares [*Kotrík et al.*, 2010; *Dohnal et al.*, 2012c]). The full and the dashed line are fits to the data at 80 K and 100 K, respectively. The horizontal dotted line is the theoretical prediction for binary recombination rate coefficient from ref. [*Pagani et al.*, 2009].

Our results confirmed existence of helium assisted three body recombination process with values of the ternary recombination rate coefficients comparable to those of H_3^+ [*Kotrík et al.*, 2010; *Dohnal et al.*, 2012c]. An example of the dependence of the measured effective recombination rate coefficient on helium number density obtained for D_3^+ ions at 80 K is shown in Figure 12. The value of the effective recombination rate coefficient linearly increases with increasing helium number density and its extrapolation to [He] = 0 is in reasonable agreement with theoretical predictions. The linear fit of the data plotted in Figure 12 ($\alpha_{eff} = \alpha_{bin} + K_{He}[He]$) yields the binary ($\alpha_{bin}$) and the ternary ($K_{He}$) recombination rate coefficients. These are plotted in Figure 13 and Figure 14, respectively.

The measured values of the binary recombination rate coefficient for D_3^+ ions are in a good agreement with theoretical predictions by Pratt and Jungen [*Pratt et al.*,

2011] while the values calculated by Kokoouline and Greene [*Pagani et al.*, 2009] are slightly larger than our data. According to private communication with V. Kokoouline [*Kokoouline*, 2012], Pratt et al. [*Pratt et al.*, 2011] used experimental data for the Jahn-Teller coupling while in the ref. [*Pagani et al.*, 2009] the couplings were theoretically calculated – the theoretical Jahn-Teller coupling constant is about 10% larger than the experimental one, which makes the recombination rate coefficient larger by about 20%.
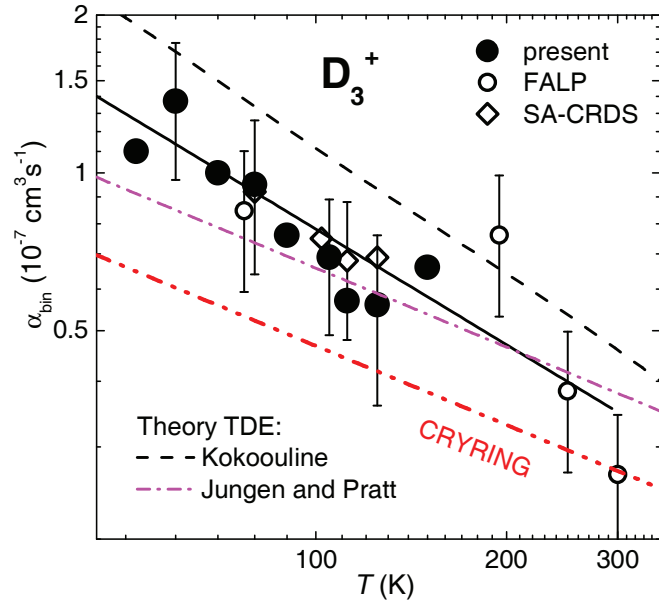
Figure 13 . Adapted from ref. [*Rubovič et al.*, 2013]. Temperature dependence of the binary recombination rate coefficients for D_3^+ ions. The values obtained in SA-CRDS (rhomboids [*Dohnal et al.*, 2012c]) and FALP (full and open circles [*Kotrík et al.*, 2010; *Rubovič et al.*, 2013]) experiments are compared to the data from ion storage ring CRYRING (double-dotted-dashed line [*Le Padellec et al.*, 1998]) and to the theoretical predictions by Kokoouline [*Pagani et al.*, 2009] and by Pratt and Jungen [*Pratt et al.*, 2011]. The full line is a fit to our FALP and SA-CRDS data.

Of particular note is the temperature dependence of the ternary recombination rate coefficient K_{He} for D_3^+ ions. It's value changes only very slowly between 100 K and 300 K but around 100 K drops significantly and then slowly increases with

decreasing temperature. We have not observed similar behaviour for H_3^+ ions (compare with data in Figure 7).
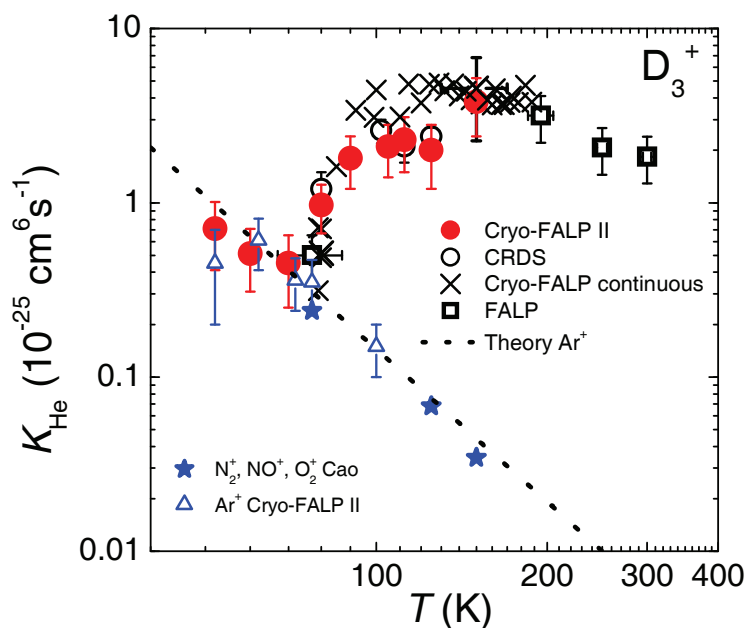
Figure 14. Adapted from ref. [*Johnsen et al.*, 2013]. Dependence of the ternary recombination rate coefficients for D_3^+ ions in helium on temperature. The data were obtained in our SA-CRDS (open circles, [*Dohnal et al.*, 2012c]) and FALP experiments (full circles, squares, crosses, see ref. [*Kotrík et al.*, 2010] and references therein). The triangles denote values of ternary recombination rate coefficient measured for Ar^+ ions in helium [*Dohnal et al.*, 2013], while the stars are ternary recombination rate coefficients reported by Cao et al. [*Cao et al.*, 1991] for a mixture of atmospheric ions in helium. Theoretical value scaled for Ar^+ ions in helium [*Bates et al.*, 1965] is plotted as dotted line.

Recombination of N_2H^+ with electrons

N_2H^+ is one of the key ions in the chemistry of interstellar medium and has been observed in a variety of environments such as translucent and dark clouds, protoplanetary disks or protostellar cores and it is used as a tracer for N_2 in dark clouds [*Turner et al.*, 1974; *Turner et al.*, 1995; *Caselli et al.*, 2002; *Anderson et al.*, 2019]. N_2H^+ is also supposed to play a role in chemistry of Titan's atmosphere [*Vuitton et al.*, 2007].

The main production pathway for N_2H^+ ions in interstellar medium is proton transfer in reaction of H_3^+ with N_2 while it is mainly destroyed in collisions with electrons (dissociative recombination) or CO molecules (proton transfer reaction).

Owing to its importance to interstellar chemistry, the dissociative recombination of N_2H^+ ions with electrons has been studied for over 40 years [*Larsson et al.*, 2008] with the results of various theoretical and experimental studies differing by almost an order of magnitude. The early merged beam study by Mul and McGowan [*Mul et al.*, 1979a] reported value of recombination rate coefficient for N_2H^+ ions at 300 K to be $\alpha = 7.5 \times 10^{-7}$ cm^{3}s^{-1} but this value should be probably divided by two due to calibration error [*Larsson et al.*, 2008]. Flowing Afterglow with Langmuir Probe (FALP) experiments obtained values ranging from 1.7×10^{-7} cm^{3}s^{-1} to 2.8×10^{-7} cm^{3}s^{-1} at 300 K [*Smith et al.*, 1984; *Adams et al.*, 1984; *Smith et al.*, 1993; *Rosati et al.*, 2004; *Poterya et al.*, 2005] while the ion storage ring CRYRING first reported the value of recombination rate coefficient at 300 K to be 1.0×10^{-7} cm^{3}s^{-1} [*Geppert et al.*, 2004] later refined upwards to 2.7×10^{-7} cm^{3}s^{-1} [*Vigren et al.*, 2012]. At lower temperatures, relevant for astrochemistry, the FALP and ion storage ring data differ by a factor of two or more. It can be expected that the rotational and vibrational populations of N_2H^+ ions in FALP experiments were in accordance with thermal equilibrium at given temperature. The rotational temperature of ions in ion storage ring was probably 300 K or higher [*Petrignani et al.*, 2011]. The only experiment with in situ identification of recombining ions was performed by Amano [*Amano*, 1990] using absorption spectroscopy with $\alpha = 7 \times 10^{-7}$ cm^{3}s^{-1} at 273 K, a value substantially higher than in other mentioned studies.

Only few theoretical studies focused on dissociative recombination of N_2H^+ ions with electrons. The direct process of dissociative recombination is highly inefficient at low energies as shown by Talbi [*Talbi*, 2007] and by Hickman et al. [*Hickman et al.*, 2011]. The indirect process was studied by Fonseca dos Santos et al. [*Fonseca dos Santos et al.*, 2014; *Fonseca dos Santos et al.*, 2016] but their results are by up to factor of two lower than the FALP or ion storage ring results and by almost order of magnitude lower than the results of Amano's experiment [*Amano*, 1990].

To resolve these discrepancies, I opted to utilize the SA-CRDS setup to probe the time evolutions of number densities of several rovibrational states of N_2H^+ ions in recombination dominated afterglow plasma to ensure that the studied ions are rotationally and vibrationally cold and the measured quantity is really thermal recombination rate coefficient.

In contrast to our previous studies on recombination of isotopomers of H_3^+ with electrons, where usable transitions were known, in case of N_2H^+ we had to find the transitions originating from the low laying rotational states in the ground and the first excited vibrational state of N_2H^+ ions. The corresponding spectroscopic study is described in ref. [*Kálosi et al.*, 2017]. Another complication has arisen due to the higher mass of N_2H^+ ion with respect to H_3^+ resulting in lower Doppler broadening and thus relatively more pronounced effect of collisional broadening. This had to be taken into account especially at higher buffer gas pressures used to estimate the influence of third bodies on measured recombination rate coefficient.

An example of measured time evolutions of number densities of several rotational states of N_2H^+ ions in the ground vibrational state is shown in Figure 15. As can be seen from Figure 15, the relative populations of different states of N_2H^+ are constant in afterglow plasma and are very close to those expected for thermal population of states. A similar picture was observed also for the first vibrationally excited state of $N_2H^+(v_1 = 0, v_2 = 1, v_3 = 0)$ with the average vibrational temperature slightly higher than the kinetic temperature of the ion T_{kin}. For details see ref. [*Shapko et al.*, 2020]. It can be thus safely assumed that the measured recombination rate coefficients correspond to N_2H^+ ions with thermal populations of rotational and vibrational states.
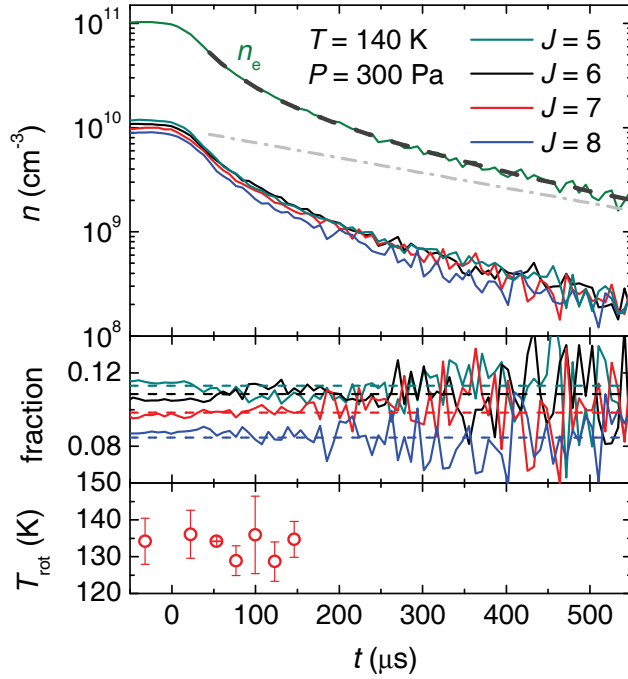
Figure 15. Adapted from ref. [*Shapko et al.*, 2020]. Upper panel: Measured time evolution of number densities of several rotational states of $N_2H^+(v_1 = 0, v_2 = 0, v_3=0)$ at 140 K, $T_{kin} = 139 \pm 6$ K, [He] $= 1.5\times10^{17}$ cm^{-3}, [Ar] $= 2.5\times10^{14}$ cm^{-3}, [H$_2$] $= 5\times10^{14}$ cm^{-3} and [N$_2$] $= 4\times10^{13}$ cm^{-3}. The electron number density, not measured in presented experiments, was calculated from the ion number densities under assumption of quasineutrality of plasma and thermal population of states. Middle panel: Time evolution of relative populations of rotational states from upper panel. Thermal populations of states are denoted by dashed lines. Lower panel: Time evolution of rotational temperature of the N$_2$H$^+$ ions in discharge and afterglow plasma.

As is the case in every experiment reported in this thesis, prior the actual measurement we employed a model of chemical kinetics to ascertain the best conditions for planned experiment. For example, at high number densities of nitrogen reactant gas the N$_4$H$^+$ ions can be formed in three body association reaction of N$_2$H$^+$ ions with N$_2$ and He:

$$N_2H^+ + N_2 + He \xrightarrow{k_{N4H}} N_4H^+ + He, \tag{39}$$
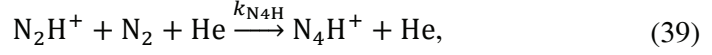
where $k_{N4H} = 2.8 \times 10^{-29}$ cm³s⁻¹ as measured at 80 K in SIFT experiment [*Adams et al.*, 1984]. Reaction (39) gives upper limit for number densities of helium and nitrogen that can be used in the experiment. This is demonstrated in Figure 16 where the measured effective recombination rate coefficient increases with increasing number density of N_2 in accordance with the prediction of the model of chemical kinetics. Note that the electron number density was not measured in these experiments. As other ions than N_2^+ are produced in the afterglow, the data evaluation procedure (see section on data analysis, equation (29)), that assumes $[N_2^+] = n_e$, gives proportionally higher value of the effective recombination rate coefficient.
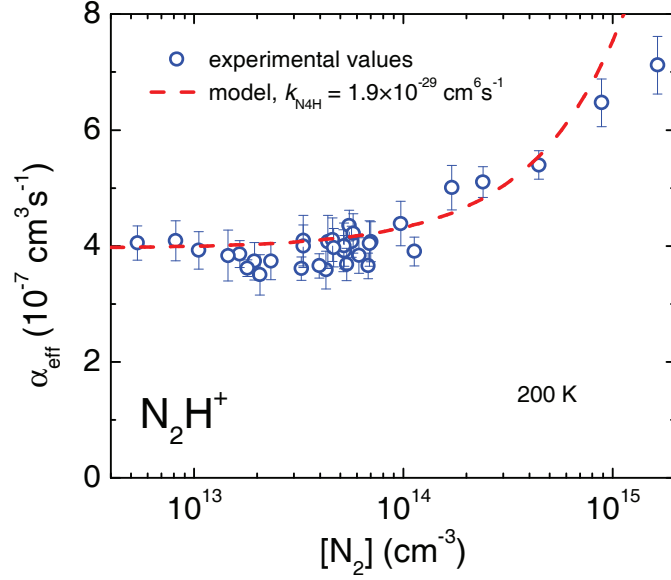
Figure 16. Adapted from ref. [*Shapko et al.*, 2020]. The dependence of the measured effective recombination rate coefficient on number density of molecular nitrogen at $T = 200 \pm 5$ K, $[He] = (1 - 5) \times 10^{17}$ cm⁻³, $[H_2] = (3 - 7) \times 10^{14}$ cm⁻³, $[Ar] \approx 5 \times 10^{14}$ cm⁻³. The dashed line denotes recombination rate coefficients obtained from the model of chemical kinetics (for details see ref. [*Shapko et al.*, 2020]).

We have seen no dependence of the measured effective recombination rate coefficient on number density of hydrogen or helium. As N_2H^+ recombines with electrons via indirect mechanism of dissociative recombination [*Fonseca dos Santos et al.*, 2014] we were interested if the ternary recombination rate coefficients for helium assisted recombination of N_2H^+ ions with electrons will be of similar magnitude as those for H_3^+ ions (and its deuterated isotopologues). As we have seen no dependence of the measured effective recombination rate coefficient on helium number density, we were only able to estimate an upper limit for N_2H^+ ternary recombination rate coefficient.
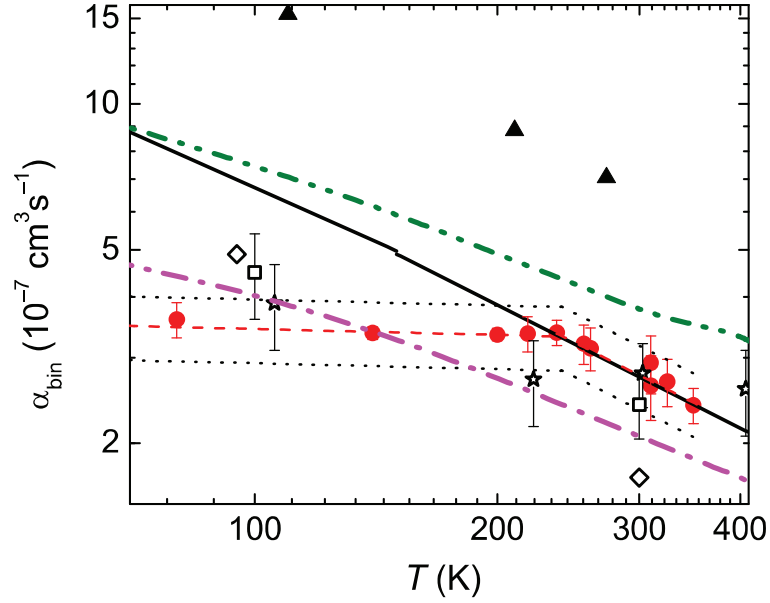
Figure 17 . Adapted from ref. [*Shapko et al.*, 2020]. The dependence of the measured recombination rate coefficient for N_2H^+ on temperature. The data were obtained in helium buffer gas with exception of the value at 350 K that was measured in hydrogen buffer gas. The recombination rate coefficients obtained in previous experiments are shown as rhomboids [*Adams et al.*, 1984], squares [*Smith et al.*, 1993], stars [*Poterya et al.*, 2005], triangles [*Amano*, 1990], double-dot-dashed line [*Mul et al.*, 1979a] and full line [*Vigren et al.*, 2012], respectively. Recent quantum mechanical predictions are plotted as dotted-dashed line [*Fonseca dos Santos et al.*, 2016]. The estimated systematic error of our data is denoted by dotted lines.

The obtained values of binary recombination rate coefficients for N_2H^+ ions are plotted in Figure 17 together with the data from experiments of other groups [*Mul et al.*, 1979a; *Adams et al.*, 1984; *Amano*, 1990; *Smith et al.*, 1993; *Poterya et al.*, 2005; *Vigren et al.*, 2012] and theoretical predictions [*Fonseca dos Santos et al.*, 2016].

As can be seen from Figure 17, there is a very good agreement between the values obtained in our SA-CRDS experiment [*Shapko et al.*, 2020] (full circles) and those from ion storage ring CRYRING [*Vigren et al.*, 2012] (full line) at 300 K but around 100 K the CRYRING values are by more than factor of two higher than the SA-CRDS data. Here it is necessary to point out one of the differences between these two experiments. In our case, the ionic rotational and vibrational populations are very close to the buffer gas temperature, in ion storage ring, the ion rotational temperature was probably 300 K [*Petrignani et al.*, 2011] even at low collisional energies. The difference between our thermal recombination rate coefficients and those from the CRYRING experiment could be an indication of higher reactivity of rotationally excited states with respect to the lower lying states. A similar effect was recently observed in recombination of HeH^+ ions with electrons [*Novotny et al.*, 2019].

Recombination of N_2^+ ions with electrons – dependence on vibrational excitation

The abilities of the Cryo-SA-CRDS setup are nicely demonstrated in our recent experiments focused on recombination of N_2^+ ions with electrons.

Molecular nitrogen is the most abundant gas in the atmosphere of the Earth and also important component of atmospheres of other large objects in solar system [*Elliot et al.*, 2000; *Krasnopolsky*, 2014; *Krasnopolsky*, 2020]. It is considered to be prevalent in ices on surfaces of trans-Neptunian objects [*Young et al.*, 2020]. This results in N_2^+ being one of the main ions in the Earth atmosphere [*Min et al.*, 2022] and in atmospheres of other solar system bodies such as Titan [*Lammer et al.*, 2020] and Triton [*Yung et al.*, 1990].

The dissociative recombination of N_2^+ ions with electrons,

$$N_2 + e^- \xrightarrow{\alpha_{N2+}} N + N,\tag{40}$$

is an important process in modelling of planetary ionospheres [*Fox et al.*, 1985; *Sheehan et al.*, 2004; *Fox*, 2005] and as such has been studied for more than 70 years both theoretically and experimentally [*Sheehan et al.*, 2004; *Larsson et al.*, 2008]. The recombination rate coefficients obtained in afterglow studies [*Kasner et al.*, 1965; *Mehr et al.*, 1969; *Zipf*, 1980; *Mahdavi et al.*, 1971; *Canosa et al.*, 1991; *Geoghegan et al.*, 1991] were limited to the temperatures of 300 K or higher with values in the range of $1.8 - 2.9 \times 10^{-7}$ $cm^3 s^{-1}$. A particular issue was observed by Zipf [*Zipf et al.*, 1980] in his stationary afterglow experiment who reported that only 87 % of N_2^+ ions were in their ground vibrational state the rest populating mainly v = 1 and v = 2 states. Johnsen [*Johnsen*, 1987] and later Bates and Mitchell [*Bates et al.*, 1991] pointed out that at conditions present in Zipf's experiment a strong resonant charge transfer process between N_2^+ ions and nitrogen molecules will take place:

$$N_2^+(v') + N_2(v = 0) \leftrightarrow N_2^+(v = 0) + N_2(v'),\tag{41}$$
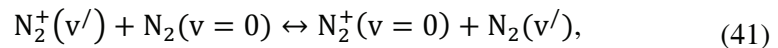
resulting in high vibrational temperature of the N_2^+ ions. Bates' reanalysis of these data also indicated that the value of the recombination rate coefficient for higher vibrational states should be lower than for the ground state [*Bates et al.*, 1991].

The results of the flowing afterglow studies [*Mahdavi et al.*, 1971; *Canosa et al.*, 1991; *Geoghegan et al.*, 1991], although performed without identification of the vibrational state of the recombinating ions, are likely pertaining to the ground vibrational state due to way how the ions are prepared in such experiments. Nevertheless, these studies were limited to 300 K partially because of fast formation of N_4^+ ions in three body association reaction of N_2^+ with helium and N_2 at low temperatures:

$$N_2^+ + N_2 + He \rightarrow N_4^+ + He. \qquad (42)$$
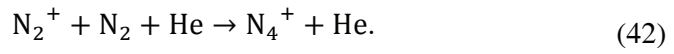
The value of the rate coefficient for reaction (42) is higher than 2×10^{-29} cm^3s^{-1} at 300 K [*Anicich et al.*, 2000].

Mul et al. [*Mul et al.*, 1979b] obtained in their merged electron – ion beam experiment value of the recombination rate coefficient $\alpha_{N2+} = 3.6\times10^{-7}$ $(T_e/300)^{-0.5}$ cm^3s^{-1} valid for electron temperatures in the range of 100 – 20 000 K (according to discussion in ref. [*Larsson et al.*, 2008] this value should be divided by a factor of two due to calibration error). Later merged electron – ion beam study by Noren et al. [*Noren et al.*, 1989] reported for vibrationally cold ions a substantially lower value of $\alpha_{N2+} = 0.4\times10^{-7}$ cm^3s^{-1} at 300 K and the value of the measured recombination coefficient increased with increasing vibrational excitation.

Ion storage ring experiment CRYRING [*Peterson et al.*, 1998] and another merged electron – ion beam study by Sheehan et al. [*Sheehan et al.*, 2004] reported practically identical cross sections in a broad energy range with inferred values of the recombination rate coefficient at 300 K of 1.75×10^{-7} cm^3s^{-1} and 1.50×10^{-7} cm^3s^{-1}, respectively. The vibrational populations of recombining ions reported by Peterson et al. [*Peterson et al.*, 1998] were 46% percent of all N_2^+ ions in the v = 0 state, 27% in v = 1, 10% in v = 2, and 16% in v = 3 state.

There are no experimental data on recombination of vibrationally cold N_2^+ ions with electrons for temperatures below 300 K.

Guberman extensively studied the collisions of N_2^+ ions with electrons using multichannel quantum defect theory [*Guberman*, 1991; *Guberman*, 2012; *Guberman*, 2014]. He predicted that at high temperatures the v = 0 state will recombine with electrons substantially faster than the vibrationally excited states. At 300 K the ratio between the recombination rate coefficients for v = 0 and v = 1 states is less than 1.5 and decreases with decreasing temperature.

Little [*Little et al.*, 2014] calculated the recombination rate coefficients for different vibrational states of N_2^+ using R matrix theory. His approach was recently refined by Abdoulanziz [*Abdoulanziz et al.*, 2021] who included in the calculation higher kinetic energies of incoming electrons and more vibrational levels of the target molecular ion. These calculations were in agreement with Guberman's predictions [*Guberman*, 2014] that the recombination process is more effective for v = 0 state of N_2^+ than for v = 1 state. On the other hand, the calculated ratio between the recombination rate coefficients for v = 0 and v = 1 states is more than 4 and does not significantly decrease with decreasing temperature. The actual value of the v = 0 recombination rate coefficient at 300 K predicted by Abdoulanziz et al. [*Abdoulanziz et al.*, 2021] is higher than that of Guberman [*Guberman* 2014], while the value for v = 1 state is substantially lower.

Based on this lengthy overview, it is clear that in order to obtain the recombination rate coefficient for N_2^+ ions in the ground vibrational state in an afterglow study, several conditions have to be fulfilled: 1) It is necessary to probe in situ the rotational and vibrational populations of the recombining ions to ensure that majority of the N_2^+ ions are in the v = 0 state. 2) Used experimental technique together with data analysis have to be able to provide reliable recombination rate coefficients even at conditions when N_2^+ ion will not be dominant ions in the afterglow due to formation of N_4^+ ions at low temperatures.

We addressed the first point by using cavity ring-down spectroscopy to probe the number densities of different rovibrational states of N_2^+ utilizing transitions originating in the ground and the first excited vibrational state (X $^2\Sigma_g^+$(v = 0) – A $^2\Pi_u$(v = 2) and X $^2\Sigma_g^+$(v = 1) – A $^2\Pi_u$(v = 3)) around 785 nm and 812 nm, respectively. Our results have shown that within the error of the measurement the rotational temperature of N_2^+ ions was very close to the wall temperature. Less than

1.5 % of all N_2^+ ions were in the v = 1 state ensuring that the measured results were pertaining to the ground vibrational state.

For the second point, the simultaneous measurement of time evolutions of N_2^+ and electron number densities enabled us to determine the recombination rate coefficients for N_2^+ (for more details on recombination rate coefficient determination at conditions when the studied ions are not dominant in afterglow plasma see discussion in Data analysis section of this thesis). An example of measured data is shown in Figure 18. The data were fitted by equation (35).
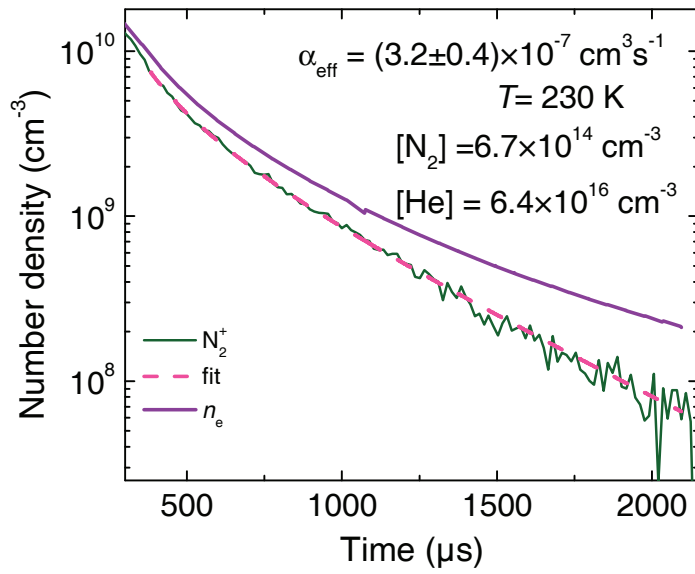
Figure 18 . Adapted from ref. [*Uvarova et al.*, 2022]. Time evolutions of measured electron and N_2^+ number densities in afterglow plasma at 230 K, [He] = 6.4×10^{16} cm^3s^{-1} and $[N_2]$ = 6.7×10^{14} cm^3s^{-1}. The dashed line is fit to the data using equation (35). The N_2^+ number density was calculated under assumption of thermal population of states from the absorption at the centre of the $Q_{22}(9.5)$ line of the $^2\Sigma_g^+$ - $^2\Pi_u$ (0 - 2) Meinel band of N_2^+.

Similar data sets as in Figure 18 were obtained for different number densities of helium and nitrogen in the temperature range of 140 – 250 K. The resulting recombination rate coefficients are plotted in Figure 19 together with values obtained in previous studies. Of particular interest is the comparison to experiments in which

the actual vibrational population of recombining ions was probed. The ion storage ring study by Peterson et al. [*Peterson et al.*, 1998] reported that more than half of the N_2^+ ions were in excited vibrational states with the corresponding recombination rate coefficient of about half of our value. The values of the recombination rate coefficient for N_2^+ ions obtained in stationary afterglow experiment by Zipf [*Zipf*, 1988], with 13 % of N_2^+ ions in excited vibrational states, are between those measured by us and by Petersen et al. [*Petersen et al.*, 1998]. Based on these data we estimated that the recombination rate coefficient for N_2^+ ions in v = 1 state at 250 K is $\alpha_{N2+(v=1)} = (4 \pm 4) \times 10^{-8}$ cm^{3}s^{-1}. For more details see ref. [*Uvarova et al.*, 2022].
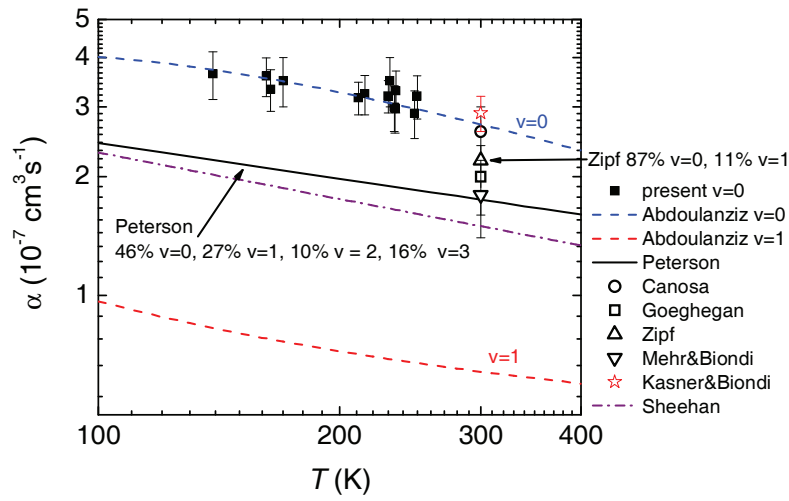
Figure 19. Adapted from ref. [*Uvarova et al.*, 2022]. Dependence of the binary recombination rate coefficient for N_2^+ ions on temperature. The values from the Cryo-SA-CRDS experiment (full squares [*Uvarova et al.*, 2022]) are compared to the data obtained in previous experimental [*Kasner et al.*, 1965; *Mehr et al.*, 1969; *Zipf*, 1988; *Canosa et al.*, 1991; *Goeghan et al.*, 1991; *Peterson et al.*, 1998; *Sheehan et al.*, 2004] and theoretical [*Abdoulanziz et al.*, 2021] studies.

Both the measured recombination rate coefficient for the vibrational ground state and the estimated value for v = 1 state are in a very good agreement with the most recent quantum mechanical calculations by Abdoulanziz et al. [*Abdoulanziz et al.*, 2021].

Dissociative recombination of N_2^+ ions with electrons is a nice example that the measured value of recombination rate coefficient can profoundly depend on the internal excitation of recombining ions.

Selected experiments in 22-pole radiofrequency ion trap

The 22-pole radiofrequency ion trap technique was developed by Dieter Gerlich in the late 20th century [*Gerlich*, 1992] and was successfully utilized for determination of reaction rate coefficients for temperatures ranging from room temperature down to below 10 K [*Gerlich*, 1995; *Gerlich et al.*, 2011; *Plašil et al.*, 2011; *Zymak et al.*, 2013; *Kumar et al.*, 2018; *Plašil et al.*, 2021].

I was lucky to work with late Dieter Gerlich during my stay in Chemnitz, Germany and then in Prague. He was a unique person both on professional and personal level.

The description of the 22-pole radiofrequency ion trap apparatus at the Department of surface and plasma science, Faculty of Mathematics and Physics of Charles University can be found e. g. in ref. [*Zymak et al.*, 2013] so only short summary will be given here. The ions are produced in a storage ion source (SIS) by electron bombardment then mass selected by passing through quadrupole mass spectrometer (QMS) and guided by ion optics to the 22-pole ion trap. After set time the trapped ions are released and after mass selection in second QMS detected using multichannel plate detector (MCP). The trap itself is connected to cold-head of a closed cycle helium refrigerator enabling operation in the range of 10 – 300 K.

The trapped ions cooled by collisions with buffer gas (usually helium) can react with added reactant gas. Reaction rate coefficients for ion – molecule reactions and product branching ratios can be determined.

I have participated on several studies involving this apparatus [*Plašil et al.*, 2011; *Plašil et al.*, 2017; *Kovalenko et al.*, 2018; *Tran et al.*, 2018; *Roučka et al.*, 2018; *Rednyk et al.*, 2019; *Rednyk et al.*, 2021; *Kovalenko et al.*, 2021; *Plašil et al.*, 2021] but I have decided to focus here on some advanced abilities of the 22-pole ion trap setup, namely to probe the internal excitation of trapped ions and to study isomer specific reaction rate coefficients and branching ratios.

The radiofrequency traps have been utilized for molecular spectroscopy for almost twenty years using schemes like laser induced reactions [*Schlemmer et al.*, 1999], laser inhibited cluster growth [*Savic et al.*, 2015] and others [*Roithová et al.*, 2019].

In our case we followed approach in ref. [*Otto et al.*, 2012] to determine the rotational temperature of OH^- ions in the trap using photodetachment spectroscopy. Light from a diode laser passed through 22-pole ion trap and the wavelength dependent rate of the decay of OH^- ions (proportional to the photodetachment cross section) was observed. An example of measured data is shown in Figure 20. The sudden increases of the photodetachment rate correspond to threshold energies for photodetachment from various rotational states of OH^- ions.
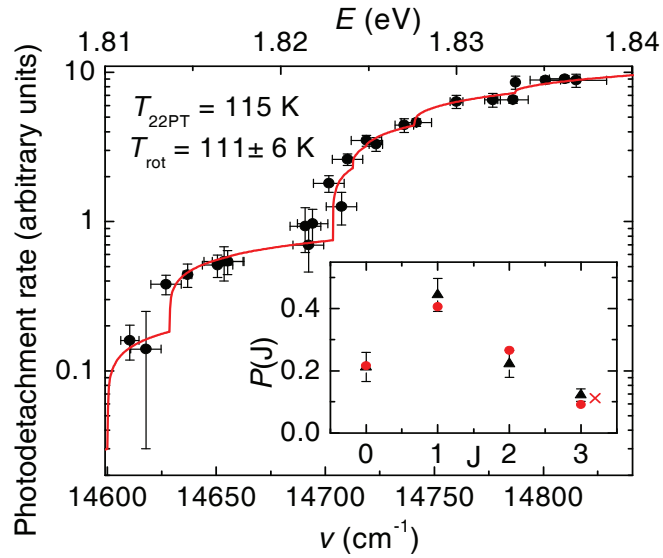
Figure 20. Adapted from ref. [*Plašil et al.*, 2022]. Photodetachment rate at trap temperature T_{22PT} = 115 K and [He] = 5.5×10^{13} cm^{-3}. The obtained rotational temperature is T_{rot} = 111 ± 6 K. The full line denotes the fit of the data under assumption of the thermal population of states with temperature as a free parameter **Insert:** The relative populations of the lowest rotational states of OH^- anion (triangles) determined from the plotted data with the populations of rotational states up to J = 3 as free parameters. The circles denote the calculated thermal populations at 115 K. The value measured for J = 3 is given by indistinguishable contributions from states with J = 3, 4, and 5 (because of the position of the corresponding photodetachment thresholds and probed wavelength range). The cross denotes the sum of the calculated relative thermal populations of these states.

The analysis of the data like those plotted in Figure 20 enables not only the calculation of the rotational temperature of trapped ions but also determination of actual populations of corresponding rotational states (see insert in Figure 20). We have shown [*Uvarova et al.*, 2021; *Plašil et al.*, 2022] that for rotational temperature measurement as few as five or six data points are sufficient. These experiments enabled us to prove that the rotational population of the ions reacting in the trap is in accordance with thermal equilibrium at given temperature in the range of 50 – 200 K. For reliable rate coefficients determination it is crucial to ensure that the reacting ions are in a well-defined state.

The second experiment, I would like to focus on, was in fact not performed in Prague but during my stay at MPE in Garching, Germany. The experimental setup is similar to that in Prague experiments differing slightly in construction of the 22-pole trap itself and in detection system (Daly detector instead of MCP). The data acquisition is based on mass selection using QMS that is not sensitive enough to distinguish between two isomers (HCN^+ and HNC^+ in this case) but can be utilized, using clever scheme, to determine the reaction rate coefficients for these ions.

A mixture of HCN^+/HNC^+ ions was prepared in storage ion source from acetonitrile or $BrCN$/H_2O precursors, then mass selected and trapped in the 22-pole radiofrequency ion trap. The actual ionic composition was monitored by reactions with SF_6 or O_2 that have different products for HCN^+ or HNC^+ [*Petrie et al.*, 1990]. The trapped ions then reacted with added H_2 gas and the reaction product were, after set trapping time, analysed by detection system consisting of QMS and Daly detector. Approximately 90 % of the trapped ions corresponding to mass 27 Dalton were HCN^+. To transform the HCN^+ to its low energy isomer HNC^+ we utilized the isomerisation reaction with CO_2 that was added to the trap [*Hansel et al.*, 1998] resulting in more than 90 % of ions at mass 27 Dalton being HNC^+.

The rate coefficients for reaction of HCN^+ with H_2 were obtained in the temperature range of 17 – 250 K and were close to Langevin reaction rate. The rate coefficients for the reaction of HNC^+ with H_2 were measured in the temperature range of 70 – 250 K (limited by freeze out of CO_2) and increased with decreasing temperature from half of Langevin reaction rate coefficient at 250 K to slightly below Langevin rate at 70 K. for both ions the product of the reaction is $HCNH^+$.

Similar approach was used for the determination of the reaction rate coefficient for the reaction of CN^+ ions with H_2 and its product branching ratios. The CN^+ ions produced in the storage ion source from $BrCN/H_2O$ were mass selected and trapped in the 22-pole radiofrequency ion trap. A short pulse of helium with H_2 admixture resulted in production of HCN^+ and HNC^+ at the beginning of the trapping period. The reaction of the produced HCN^+ and HNC^+ with SF_6 was utilized to determine the product branching ratios. The reaction rate coefficient for reaction of CN^+ with H_2 was determined in the range of 17 – 250 K, while the branching ratios were measured only for temperatures above 90 K (due to freeze out of SF6).

The results are summarized in Figure 21 and are prepared for publication.
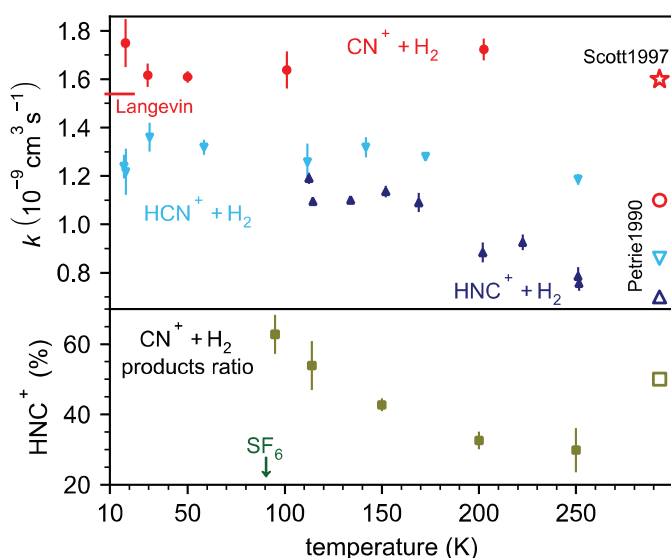
Figure 21. Adapted from ref. [*Dohnal et al.*, 2022]. Reaction rate coefficients for reactions of CN^+ (red), HCN^+ (cyan) and HNC^+ (dark blue) ions with H_2 (top) and branching ratio for the $CN^+ + H_2$ reaction (bottom). Open symbols denote values from previous studies (star [*Scott et al.*, 1997], the rest from ref. [*Petrie et al.*, 1991]). The Langevin reaction rate coefficient for reaction of CN^+ ions with H_2 is 1.54×10^{-9} $cm^3 s^{-1}$. Green down arrow points to the freezeout temperature of SF_6 that was used for branching ratio determination.

Conclusions

This thesis summarized years of studies of recombination of atomic and molecular ions with electrons performed in afterglow plasma using several experimental techniques. I focused on the influence of collisions with third bodies on the recombination process and on the possible different reactivity of different quantum states of ions.

I gradually realized that in order to obtain reliable recombination rate coefficients it is necessary characterize in detail the recombining ions – their internal excitation – and also the environment in which the recombination takes places. This is of course very time consuming – it took approximately two years to obtain data on N_2H^+ recombination with electrons [*Shapko et al.*, 2020]. The determination of H_2D^+ and HD_2^+ [Dohnal et al., 2016; *Plašil et al.*, 2017] recombination rate coefficients was even more demanding. But it is a necessary sacrifice as otherwise we would be blind to possible effects of for example vibrational excitation of recombining ions as was the case in many previous experiments on N_2^+ recombination [*Uvarova et al.*, 2022].

This meticulous approach to recombination studies is supported by advances in instrumentation. After several low temperature FALP modifications, we developed a cryogenic stationary afterglow apparatus (Cryo-SA-CRDS) enabling recombination studies in the range of $30 - 300$ K with different diagnostic techniques [*Plašil et al.*, 2018; *Shapko et al.*, 2021].

We are now in a unique position. Our present experimental equipment and years of experience in recombination studies are coming to fruit as now we are able to study recombination of a large scale of ions not limited by the necessity of them being dominant specie in afterglow plasma and with resolution of particular quantum states (see discussion in section on N_2^+ recombination and in refs. [*Shapko et al.*, 2021; *Uvarova et al.*, 2022]).

As stated in a famous misquote of Shakespeare, the future is the undiscovered country.

References

Abdoulanziz A., Argentin C., Laporta V., Chakrabarti K., Bultel A., Tennyson J., Schneider I. F., Mezei J. Zs.: *J. Appl. Phys.* **129**, 053303, 2021.

Adams N. G., Smith D., Alge E.: *J. Chem. Phys.* **81**, 1778, 1984.

Adams N. G., Smith D.: in *Dissociative Recombination, Theory, Experiment and Application*, ed. by J. B. A. Mitchell, S. L. Guberman, World Scientific, Singapore, 29, 1989.

Albertsson T., Semenov D. A., Vasyunin A. I., Henning T. Herbst E.: *Astrophys. J. Suppl. Ser.* **207**, 27, 2013.

Albertsson T., Indriolo N., Kreckel H., Semenov D., Crabtree K. N., Henning T.: *Astrophys. J.* **787**, 44, 2014.

Amano T.: *J. Chem. Phys.* **92**, 6492, 1990.

Anderson D. Z., Frisch J. C., Masser C. S.: *Appl. Opt.* **23**, 1238, 1984.

Anderson D. E., Blake G. A., Bergin E. A., Zhang K., Carpenter J. M., Schwartz K. R., Huang J., Oberg K. I.: *Astrophys. J.* **881**, 127, 2019.

Anicich V. G., Milligan D. B., Fairley D. A., McEwan M. J.: *Icarus* **146**, 118-124, 2000.

Auerbach D., Cacak R., Caudano R., Gaily T. D., Keyser C. J., McGowan J. W., Mitchell J. B. A., Wilk S. F. J.: *J. Phys. B* **10**, 3797, 1977.

Bannasch G., Pohl T.: *Phys. Rev. A* **84**, 052710, 2011.

Bates D. R., Massey H. S. W.: *Proc. Roy. Soc. A* **192**, 1, 1947.

Bates D. R.: *Phys. Rev.* **78**, 492, 1950.

Bates D. R., Kingston A. E., McWhirter R. W. P.: *Proc. R. Soc. A* **267**, 297, 1962.

Bates D. R., Khare S. P.: *Proc. Phys. Soc.* **85**, 231, 1965.

Bates D. R., Mitchell J. B. A.: *Planet. Space. Sci.* **39**, 1297, 1991.

Beer A.: *Annalen der Physik und Chemie* **86**, 78, 1852.

Berden G., Engeln R. (editors): *Cavity Ring-Down Spectroscopy: Techniques and Applications*. Wiley-Blackwell, 2009.

Berlande J., Cheret M., Deloche R., Gonfalone A., Manus C.: *Phys. Rev. A* **1**, 887, 1970.

Bernath P. F.: *Spectra of Atoms and Molecules*. Oxford University Press, Oxford, 2005.

Biondi M. A., Brown S. C.: *Phys. Rev.* **75**, 1700, 1949a.

Biondi M. A., Brown S. C.: *Phys. Rev.* **76**, 1697, 1949b.

Brown S. C., Rose D. J.: *J. Appl. Phys.* **23**, 711, 1952.

Canosa A., Gomet J. C., Rowe B. R., Queffelec J. L.: *J. Chem. Phys.* **94**, 7150, 1991.

Canosa A., Gomet J. C., Rowe B. R., Mitchell J. B. A., Queffelec J. L., *J. Chem. Phys.* **97**, 1028, 1992.

Cao Y. S., Johnsen R.: *J. Chem. Phys.* **94**, 5443, 1991.

Caselli P., Walmsley C. M., Zucconi A., Tafalla M., Dore L., Myers P. C.: *Astrophys. J.* **565**, 344, 2002.

Curry B. P.: *Phys. Rev. A* **1**, 166, 1970.

Das A., Majumdar L., Chakrabarti S. K., Sahu D.: *New Astron.* **35**, 53, 2015.

Datz S., Larsson M., Stromholm C., Sundstrom H., Zengin V., Danared H., Kallberg A., Ugglas M.: *Phys. Rev. A* **52**, 2901, 1995.

Deloche R., Monchicourt P., Cheret M., Lambert F.: *Phys. Rev. A* **13**, 1140, 1976.

Dohnal P., Hejduk M., Varju J., Rubovič P., Roučka Š., Kotrík T., Plašil R., Glosík J., Johnsen R.: *J. Chem. Phys.* **136**, 244304, 2012a.

Dohnal P., Hejduk M., Varju J., Rubovič P., Roučka Š., Kotrík T., Plašil R., Johnsen R., Glosík J.: *Philos. Trans. R. Soc. A − Math. Phys. Eng. Sci.* **370**, 5101, 2012b.

Dohnal P., Hejduk M., Rubovič P., Varju J., Roučka Š., Plašil R., Glosík J.: *J. Chem. Phys.* **137**, 194320, 2012c.

Dohnal P.: *Ph.D. Thesis*, Charles University, Prague, 2013.

Dohnal P., Rubovič P., Kotrík T., Hejduk M., Plašil R., Johnsen R., Glosík J.: *Phys. Rev. A* **87**, 052716, 2013.

Dohnal P., Rubovič P., Kálosi Á., Hejduk M., Plašil R., Johnsen R., Glosik J.: *Phys. Rev. A* **90**, 042708, 2014.

Dohnal P., Kálosi Á., Plašil R., Roučka Š., Kovalenko A., Rednyk S., Johnsen R., Glosík J.: *Phys. Chem. Chem. Phys.* **18**, 23549, 2016.

Dohnal P., Shapko D., Kálosi Á., Kassayová M., Roučka Š., Rednyk S., Plašil R., Hejduk M., Glosík J.: *Faraday Discuss.* **217**, 220, 2019.

Dohnal P., Jusko P., Jimenez-Redondo M., Caselli P.: Isomer specific reactions of CN^+, HCN^+ and HNC^+ with H_2, *manuscript is being prepared for publication.*

van der Donk P., Yousif F. B., Mitchell J. B. A.: *Phys. Rev. A* **43**, 5971, 1991.

Elliot J. L., Strobel D. F., Zhu X., Stansberry J. A., Wasserman L. H., Franz O. G.: *Icarus* **143**, 425, 2000.

Feher M., Rohrbacher A., Maier J. P.: *Chem. Phys.* **185**, 357, 1994.

Fehsenfeld F. C., Ferguson E. E., Schmeltekopf A. L.: *J. Chem Phys.* **44(8)**, 3022, 1966.

Ferguson E. E., Fehsenfeld F. C., Schmeltekopf A. L.: *Adv. At. Mol. Phys.* **5**, 1, 1969.

Flannery M. R.: *J. Chem. Phys.* **95**, 8205, 1991.

Fonseca dos Santos S., Kokoouline V., Greene C. H.: *J. Chem. Phys.* **127**, 124309, 2007.

Fonseca dos Santos S., Douguet N., Kokoouline V., Orel A. E.: *J. Chem. Phys.* **140**, 164308, 2014.

Fonseca dos Santos S., Ngassam V., Orel A. E., Larson A.: *Phys. Rev. A* **94**, 022702, 2016.

Fox J. L., Dalgarno A.: *J. Geophys. Res.: Space Phys.* **90**, 7557, 1985.

Fox, J. L.: *J. Phys.: Conf. Ser.* **4**, 32, 2005.

Geballe T. R., Oka T., *Nature* **384**, 334, 1996.

Geppert W., Thomas R., Semaniak J., Ehlerding A., Millar T. J., Osterdahl F., af Ugglas M., Djuric N., Paal A., Larsson M.: *Astrophys. J.* **609**, 459, 2004.

Gerbev S.: *J. Phys. B: At. Mol. Opt. Phys.* **51**, 035008, 2018.

Gerlich D.: *Adv. Chem. Phys.* **82**, 594, 1992.

Gerlich D.: *Phys. Scr.* **1995**, 256, 1995.

Gerlich D., Borodi G., Luca A., Mogo C., Smith M. A.: *Z. Für Phys. Chem.* **225**, 475, 2011.

Glosík J., Plašil R., Poterya V., Kudrna P., Tichý M.: *Chem. Phys. Lett.* **331**, 209, 2000.

Glosík J., Novotný O., Pysanenko A., Zakouřil P., Plašil R., Kudrna P., Poterya V.: *Plasma Sources Sci. Technol.* **12**, S117, 2003.

Glosík J., Korolov I., Plašil R., Novotný O., Kotrík, T, Hlavenka P., Varju J., Mikhailov I. A., Kokoouline V., Greene C. H.: *J. Phys. B-At. Mol. Opt. Phys.* **41**, 191001, 2008.

Glosík J., Plašil R., Korolov I., Kotrík T., Novotný O., Hlavenka P., Dohnal P., Varju J., Kokoouline V., Greene C. H.: *Phys. Rev. A* **79**, 052707, 2009.

Glosik J., Dohnal P., Rubovič P., Kálosi Á., Plašil R., Roučka Š., Johnsen R.: *Plasma Sources Sci. Technol.* **24**, 065017, 2015.

Goeghegan M., Adams N. G., Smith D.: *J. Phys. B At. Mol. Opt. Phys.* **24**, 2589, 1991.

Gougousi T., Johnsen R., Golde M. F.: *Int. J. Mass Spectrom.* **149-150**, 131, 1995.

Guberman, S. L.: *Geophys. Res. Lett.* **18**, 1051, 1991.

Guberman, S. L.: *J. Chem. Phys.* **137**, 074309, 2012.

Guberman, S. L.: *J. Chem. Phys.* **141**, 204307, 2014.

von Hahn R., Becker A., Berg F., et al.: *Rev. Sci. Instrum.* **87**, 063115, 2016.

Hansel A., Glantschnig M., Scheiring C., Lindinger W., Ferguson E. E.: *J. Chem. Phys.* **109**, 1743, 1998.

Hejduk M., Dohnal P., Rubovič P., Kálosi Á., Plašil R., Johnsen R., Glosík J.: *J. Chem. Phys.* **143**, 044303, 2015.

Herbelin J. M., McKay J. A., Kwok M. A., Ueunten R. H., Urevig D. S., Spencer D. J., Benard D. J.: *Appl. Opt.* **19**, 144, 1980.

Herbst E., Klemperer W.: *Astrophys. J.* **185**, 505, 1973.

Hickman A. P., Kashinski D. O., Malenda R. F., Gatti F., Talbi D.: *J. Phys. Conf. Ser.* **300**, 012016, 2011.

Hugo, E., Asvany O., Schlemmer S.: *J. Chem. Phys.* **130**, 164302, 2009.

Hus H., Yousif F., Sen A., Mitchell J. B. A.: *Phys. Rev. A* **38**, 658, 1988.

Hutchinson I. H.: *Principles of Plasma Diagnostics*, Cambridge University Press, Cambridge, 2002.

Jensen M. J., Pedersen H. B., Safvan C. P., Seiersen K., Urbain X., Andersen L. H.: *Phys. Rev. A* **63**, 052701, 2001.

Jiang P., Guthrie J., Roberts J. L.: *Phys. Plasmas* **27**, 012109, 2020.

Johnsen R.: *Int. J. Mass Spectrosc. Ion Processes* **81**, 67, 1987.

Johnsen R., Rubovič P., Dohnal P., Hejduk M., Plašil R., Glosík J.: *J. Phys. Chem. A* **117**, 9477, 2013.

Johnson A. W., Gerardo J. B.: *Phys. Rev. Lett.* **27**, 835, 1971.

Jungen C., Pratt S. T.: *Phys. Rev. Lett.* **102**, 023201, 2009.

Kálosi Á., Dohnal P., Augustovičová L., Roučka Š., Plašil R., Glosík J.: *Eur. Phys. J.-Appl. Phys.* **75**, 24707, 2016.

Kálosi Á., Dohnal P., Shapko D., Roučka Š., Plašil R., Johnsen R., Glosík J.: *J. Instrum.* **12**, C10010, 2017.

Kasner W. H., Biondi M. A.: *Phys. Rev.* **137**, A317, 1965.

Killian T. C., Kulin S., Bergeson S. D., Orozco L. A., Orzel C., Rolston S. L.: *Phys. Rev. Lett.* **83**, 4776, 1999.

Kokoouline V., Greene C. H., Esry B. D.: *Nature* **412**, 891, 2001.

Kokoouline V.: Private communication, 2012.

Korolov I., Kotrík T., Plašil R., Varju J., Hejduk M., Glosík J.: *Contrib. Plasma Phys.* **48**, 521, 2008.

Korolov I., Plašil R., Kotrík T., Dohnal P., Glosík J.: *Int. J. Mass Spectrom.* **280**, 144, 2009.

Kotrík T., Dohnal P., Korolov I., Plašil R., Roučka Š., Glosík J., Greene C. H., Kokoouline V.: *J. Chem. Phys.* **133**, 034305, 2010.

Kotrík T., Dohnal P., Roučka Š., Jusko P., Plašil R., Glosík J., Johnsen R.: *Phys. Rev. A* **83**, 032720, 2011a.

Kotrík T., Dohnal P., Rubovič P., Plašil R., Roučka Š., Opanasiuk S., Glosík J.: *Eur. Phys. J. Appl. Phys.* **56**, 24011, 2011b.

Kotrík T.: Electron-Ion Recombination at Temperatures below 300 K: *Ph.D. Thesis*, Charles University in Prague, Czech Republic, 2013.

Kovalenko A., Tran T. D., Rednyk S., Roučka Š., Dohnal P., Plašil R., Gerlich D., Glosík J.: *Astrophys. J.* **856**, 100, 2018.

Kovalenko A., Roučka Š., Tran T. D., Rednyk S., Plašil R., Dohnal P., Glosík J.: *J. Chem. Phys.* 154, 094301, 2021.

Krasnopolsky V. A.: *Icarus* **236**, 83, 2014.

Krasnopolsky V. A.: *Icarus* **335**, 113374, 2020.

Kreckel H., Novotný O., Crabtree K. N., Buhr H. et al.: Phys. Rev. A 82, 042715, 2010.

Kumar S. S., Grussie F., Suleimanov Y. V., Guo H., Kreckel H. Sci. Adv. 4, eaar3417, 2018.

Lammer H., Stumptner W., Molina-Cuberos G., Bauer S., Owen T.: *Planet. Space Sci.* **48**, 529, 2000.

Lammich L., Strasser D., Kreckel H., Lange M., Pedersen H. B., Altevogt S., Andrianarijaona V., Buhr H., Heber O., Witte P., Schwalm, D., Wolf A., Zajfman D.: *Phys. Rev. Lett.* **91**, 143201, 2003.

Langmuir I.: *J. Franklin Inst.* **196**, 751, 1923.

Larsson M., Danared H., Larson A., Le Padellec A., Peterson J. R., Rosén S., Semaniak J., Stromholm C.: *Phys. Rev. Lett.* **79**, 395, 1997.

Larsson M., Orel A. E.: *Dissociative Recombination of Molecular Ions*. Cambridge University Press, Cambridge, 2008.

Laube S., Padellec A. L., Sidko O., Rebrion-Rowe C., Mitchell J. B. A., Rowe B. R.: *J. Phys. B* **31**, 2111, 1998.

Lehmann K. K., Romanini D.: *J. Chem. Phys.* **105**, 10263, 1996.

Le Padellec A., Larsson M., Danared H., Larson A., Peterson J. R., Semaniak J., Stromholm C.: *Phys. Scr.* **57**, 215, 1998.

Leu M., Biondi M. A., Johnsen R.: *Phys. Rev. A* **8**, 413, 1973.

Little D. A., Chakrabarti K., Mezei Zs., Schneider I. F., Tennyson, J.: *Phys. Rev. A* **90**, 052705, 2014.

MacDonald J. A., Biondi M. A., Johnsen R.: *Planet. Space Sci.* **32**, 651, 1984.

Macko P., Bano G., Hlavenka P., Plašil R., Poterya V., Pysanenko A., Votava O., Johnsen R., Glosík J.: *Int. J. Mass Spectrom.* **233**, 299, 2004.

Mahdavi M. R., Hasted J. B., Nakshbandi M. M.: *J. Phys. B: At. Mol. Phys.* **4**, 1726, 1971.

Mansbach P., Keck J.: *Phys. Rev.* **181**, 275, 1969.

Mathur D., Khan S. U., Hasted J. B.: *J. Phys. B* **11**, 3615, 1978.

McCall B. J., Honeycutt A. J., Saykally R. J., Djuric N., Dunn G. H., Semaniak J., Novotný O., Al-Khalili A., Ehlerding A., Hellberg F., Kalhori S., Neau A., Thomas R. D., Paal A., Osterdahl F., Larsson M.: *Phys. Rev. A* **70**, 052716, 2004.

McGowan J. W., Mul P. M., D'Angelo V. S., Mitchell J. B. A., Defrance P., Froelich H. R.: *Phys. Rev. Lett.* **42**, 373, 1979.

McGuyer B. H., McDonald M., Iwata G. Z., Tarollo M. G., Grier A. T., Apfelbeck F., Zelevinsky T.: New J. Phys. **17**, 055004, 2015.

Mehr F. J., Biondi M. F.: *Phys. Rev.* **181**, 264, 1969.

Millar T. J.: *Astron. Geophys.* **46**, 2.29, 2005.

Millar T. J.: *Plasma Sources Sci. Technol.* **24**, 043001, 2015.

Min M.-Y., Ilie R.: *Front. Astron. Space Sci.* **8**, 745357, 2022.

Mitchell J. B. A., Ng C. T., Janssen F. L., McGowan J. W.: *J. Phys. B: At. Mol. Phys.* **17**, L909, 1984.

Morville J.: Injection des cavits optiques de haute finesse par laser a diode – Application a la CW-CRDS et a la detection de traces atmospheriques, *Ph.D. Thesis*, L'Universit Joseph Fourier – Grenoble I, France, 2001.

Mott-Smith H. M., Langmuir I.: *Phys. Rev.* **28**, 727, 1926.

Mul P. M., McGowan J. W.: *Astrophys. J. Lett.* **227**, L157, 1979a.

Mul P. M., McGowan J. W.: *J. Phys. B At. Mol. Opt. Phys.* **12**, 1591, 1979b.

Noren C., Yousif F. B., Mitchell J. B. A.: *J. Chem. Soc. Faraday Trans.* **2**, 85, 1697, 1989.

Novotný O., Plašil R., Pysanenko A., Korolov I., Glosík J.: *J. Phys. B* **39**, 2561, 2006.

Novotný O., Wilhelm P., Paul D., Kálosi Á., Saurabh S., Becker A., Blaum K., George S., Gock J., Wolf A.: *Science* **365**, 676, 2019.

Oka T.: *Proc. Natl. Acad. Sci. U. S. A.* **103**, 12235, 2006.

O'Keefe A., Deacon D. A. G.: *Rev. Sci. Instrum.* **59**, 2544, 1988.

Otto R., von Zastrow A., Best T., Wester R.: *Phys. Chem. Chem. Phys.* **15**, 612, 2013.

Pagani L., Vastel C., Hugo E., Kokoouline V., Greene C. H., Bacmann A., Bayet E., Ceccarelli C., Peng R., Schlemmer S.: *Astron. Astrophys.* **494**, 623, 2009.

Parise B., Belloche A., Du F., Gunsten R., Menten K. M.: *Astron. Astrophys.* 526, A31, 2011.

Peart B., Dolder K. T.: *J. Phys. B* **7**, 1948, 1974.

Persson K. B., Brown S.: *Phys. Rev.* **100**, 729, 1955.

Peterson J. R., Le Padellec A., Danared H., et al.: *J. Chem. Phys.* **108**, 1978, 1998.

Petrie S., Freeman C. G., Meot-Ner M., McEwan M. J., Ferguson E. E., J. Am. Chem. Soc. **112**, 7121, 1990.

Petrie S., Freeman G., McEwan M. J., Ferguson E. E.: *Mon. Notices Royal Astron. Soc.* 248, 272, 1991.

Petrignani A., Altevogt S., Berg M. H., et al., *Phys. Rev. A* **83**, 032711, 2011.

Pfau S., Tichý M.: in *Low Temperature Plasma Physics*, ed. by R. Hippler, Wiley-VCH, 131, 2001.

Pitaevskii L. P.: *Sov. Phys.-JETP* **1**, 919, 1962.

Plašil R., Glosík J., Poterya V., Kudrna P., Rusz J., Tichý M., Pysanenko A.: *Int. J. Mass Spectrom.* **218**, 105, 2002.

Plašil R., Mehner T., Dohnal P., Kotrík T., Glosík J., Gerlich D.: *Astrophys. J.* **737**, 60, 2011.

Plašil R., Dohnal P., Kálosi Á., Roučka Š., Johnsen R., Glosík J.: Plasma Sources Sci. Technol. 26, 035006, 2017.

Plašil R., Tran T. D., Roučka Š., Jusko P., Mulin D., Zymak I., Rednyk S., Kovalenko A., Dohnal P., Glosík J., Houfek K., Táborský J., Čížek M.: *Phys. Rev. A* **96**, 062703, 2017.

Plašil R., Dohnal P., Kálosi Á., Roučka Š., Shapko D., Rednyk S., Johnsen R., Glosík J.: *Rev. Sci. Instrum.* **89**, 063116, 2018.

Plašil R., Rednyk S., Kovalenko A., Tran T. D., Roučka Š., Dohnal P., Novotný O., Glosík J.: *Astrophys. J.* **910**, 155, 2021.

Plašil R., Rednyk S., Roučka Š., Uvarova L., Vanko E., Dohnal P., Glosík J.: The temperature dependence of the rate coefficient of reaction of OH⁻ anion with HD at temperatures from 20 K up to 300 K. Experimental study using RF 22-Pole Ion Trap, *manuscript is being prepared for publication.*

Pohl T., Vrinceanu D., Sadeghpour H. R.: *Phys. Rev. Lett.* **100**, 223201, 2008.

Poterya V., Glosik J., Plasil R., Tichy M., Kudrna P., Pysanenko A.: *Phys. Rev. Lett.* **88**, 044802, 2002.

Poterya V., McLain J. L., Adams N. G., Babcock L. M.: *J. Phys. Chem. A* **109**, 7181, 2005.

Pratt S. T., Jungen C.: *J. Phys.: Conf. Ser.* **300**, 012019, 2011.

Rednyk S., Roučka Š., Kovalenko A., Tran T. D., Dohnal P., Plašil R., Glosík J.: *Astron. Astrophys.* **625**, A74, 2019.

Rednyk S., Roučka Š., Dohnal P., Hejduk M., Glosík J., Plašil R.: *Phys. Rev. A* **104**, 062803, 2021.

Rennick C. J., Saquet N., Morrison J. P., Ortega-Arroyo J., Godin P., Fu L., Schulz-Weiling M., Grant E. R.: *J. Phys.: Conf. Ser.* **300**, 012005, 2011.

Richardson J. M., Holt R. B.: *Phys. Rev.* **81**, 153, 1951.

Roberts H., Herbst E., Millar T. J.: *Astron. Astrophys.* **424**, 16, 2004.

Roithova J., Jašík J., Del Pozo Mellado J., Gerlich D.: *Faraday Discuss.* **217**, 98, 2019.

Romanini D., Kachanov A. A., Stoeckel F.: *Chem. Phys. Lett.* **270**, 546, 1997.

Rosati R. E., Johnsen R., Golde M. F.: *J. Chem. Phys.* **120**, 8025, 2004.

Roučka Š., Rednyk S., Kovalenko A., Tran T. D., Plašil R., Kálosi Á., Dohnal P., Gerlich D., Glosík J.: *Astron. Astrophys.* **615**, L6, 2018.

Rubovič P., Dohnal P., Hejduk M., Plašil R., Glosík J.: *J. Phys. Chem. A* **117**, 9626, 2013.

Savic I., Gerlich D., Asvany O., Jusko P., Schlemmer S.: *Mol. Phys.* **113**, 2320, 2015.

Schippers S., Lestinsky M., Muller A., Savin D. W., Schmidt E. W., Wolf A.: *International Review of Atomic and Molecular Physics (IRAMP)* **1**, 109, 2010.

Schlemmer S., Kuhn T., Lescop E., Gerlich D.: *Int. J. Mass Spectrom.* **185**, 589, 1999.

Schregel C. G., Carbone E. A. D., Luggenholscher D., Czarnetzki U.: *Plasma Sources Sci. Technol.* **25**, 054003, 2016.

Scott G. B., Fairley D. A., Freeman C. G., McEwan M. J., Spanel P., Smith D.: *J. Chem. Phys.* **106**, 3982, 1997.

Shapko D., Dohnal P., Kassayová M., Kálosi Á., Rednyk S., Roučka Š., Plašil R., Augustovičová L. D., Johnsen R., Špirko V., Glosík J.: *J. Chem. Phys.* **152(2)**, 024301, 2020.

Shapko D., Dohnal P., Roučka Š., Uvarova L., Kassayová M., Plašil R., Glosík J.: *J. Mol. Spectrosc.* **378**, 111450, 2021.

Sheehan C. H., St.-Maurice J. P.: *J. Geophys. Res.* **109**, A03302, 2004.

Sipila O., Caselli P., Harju J.: *Astron. Astrophys.* **554**, A92, 2013.

Skrzypkowski M. P., Johnsen R., Rosati R. E., Golde M. F.: *Chem. Phys.* **296(1)**, 23, 2004.

Smith J. R., Hershkowitz N., Coakley P.: *Rev. Sci. Instrum.* **50**, 210, 1979.

Smith D., Adams N. G.: *Astrophys. J. Lett.* **284**, L13, 1984.

Smith D., Španěl P.: *Int. J. Mass Spectrom. Ion Processes* **129**, 163, 1993.

Strasser D., Lammich L., Kreckel H., Lange M., Krohn S., Schwalm D., Zajfman D.: *Phys. Rev. A* **69**, 064702, 2004.

Stevefelt J., Boulmer J., Delpech J.: *Phys. Rev. A* **12**, 1246, 1975.

Sundstrom G., Mowat J. R., Danared H., Datz S., Brostrom L., Filevich A., Kallberg A., Mannervik S., Rensfel K. G., Sigray P., af Ugglas M., Larsson M.: *Science* **263**, 785, 1994.

Šícha M., Gajdůšek J., Vepřek Š.: *Br. J. Appl. Phys.* **17**, 1511, 1966.

Talbi D.: *Chem. Phys.* **332**, 298, 2007.

Tanabe T., Chida K., Watanabe T., Arakaki Y., Takagi H., Katayama I., Haruyama Y., Saito M., Nomura I., Honma T., Noda K., Hoson K.: in *Dissociative Recombination, Theory, Experiment and Applications IV*, ed. by M. Larsson, J. B. A. Mitchell, I. F. Schneider, World Scientific, Singapore, 170, 1999.

Tennyson J., Miller S.: *Spectrochim. Acta A* **57**, 661, 2001.

Thomson J. J.: *Phil. Mag.* **47**, 337, 1924.

Tom B. A., Zhaunerchyk V., Wiczer M. B., et al.: *J. Chem. Phys.* **130**, 031101, 2009.

Torrisi G., Naselli E., Donato L. D., Mauro G. S., Mazzaglia M., Mishra B., Pidatella A., Sorbello G., Mascali D.: *J. Instrum.* **17**, C01050, 2022.

Tran T. D., Rednyk S., Kovalenko A., Roučka Š., Dohnal P., Plašil R., Gerlich D., Glosík J.: *Astrophys. J.* **854**, 25, 2018.

Turner B. E.: *Astrophys. J. Lett.* **193**, L83, 1974.

Turner B. E.: *Astrophys. J.* **449**, 635, 1995.

Uvarova L., Dohnal P., Kasayová M., Rednyk S., Roučka Š., Plašil R., Glosík J.: Recombination of vibrationally cold N_2^+ ions with electrons, *prepared for publication in J. Geophys. Res. (Atmos)*.

Varnerin, Jr. L. J.: *Phys. Rev.* **84**, 563, 1951.

Vigren E., Zhaunerchyk V., Hamberg M., Kaminska M., Semaniak J., af Ugglas M., Larsson M., Thomas R. D., Geppert W. D.: *Astrophys. J.* **757**, 34, 2012.

Vorob'ev V. S.: *Phys. Plasmas* **24**, 073513, 2017.

Vuitton V., Yelle R. V., McEwan M. J.: *Icarus* **191**, 722, 2007.

Wojcik M., Tachiya M.: *J. Chem. Phys.* **110**, 10016, 1999.

Wojcik M., Tachiya M.: *J. Chem. Phys.* **112**, 3845, 2000.

Wolz T., Malbrunot C., Vieille-Grosjean M., Comparat D.: *Phys. Rev. A* **101**, 043412, 2020.

Yariv A.: *Optical Electronics in Modern Communications*, 5rd ed., Oxford University Press, Oxford, 1997.

Yung Y. L., Lyons J. R.: *Geophys. Res. Lett.* **17**, 1717, 1990.

Young L. A., Braga-Ribas F., Johnson R. E.: Volatile evolution of atmospheres of trans-neptunian objects", in *The Trans-Neptunian Solar System*, ed. by D. Prialnik, M. A. Barucci, L. A. Young, Elsevier, The Netherlands, 2020, Chapter 6, p. 127.

Zhaunerchyk V., Thomas R. D., Geppert W. D., Hamberg M., Kaminska M., Vigren E., Larsson M.: *Phys. Rev. A* **77**, 034701, 2008.

Zipf E. C.: *Geophys. Res. Lett.* **7**, 645, 1980.

Zymak I., Hejduk M., Mulin D., Plasil R., Glosik J., Gerlich D.: *Astrophys. J.* **768**, 86, 2013.

List of publications

Publications in journals with impact factor

1) **Cavity ring-down spectroscopy study of neon assisted recombination of H_3^+ ions with electrons**
Shapko, D., Dohnal, P., Roučka, Š., Uvarova, L., Kassayová, M., Plašil, R., Glosík, J.,
J. Mol. Spectrosc. **378**, 111450, 2021.

2) **Reaction of carbon dication C_2^+ with O_2, N_2, CO, and HD at low temperatures: Experimental study using a 22-pole ion trap**
Rednyk, S., Roučka, Š., Dohnal, P., Hejduk, M., Glosík, J., Plašil, R.,
Phys. Rev. A **104(6)**, 062803, 2021.

3) **The reaction of $O^+(4S)$ ions with H_2, HD, and D_2 at low temperatures: Experimental study of the isotope effect**
Kovalenko, A., Roučka, Š., Tran, T. D., Rednyk, S., Plašil, R., Dohnal, P., Glosík, J.,
J. Chem. Phys. **154(9)**, 094301, 2021.

4) **Experimental Study on CH^+ Formation from Doubly Charged Carbon and Molecular Hydrogen**
Plašil, R., Rednyk, S., Kovalenko, A., Tran, T. D., Roučka, Š., Dohnal, P., Novotný, O., Glosík, J.,
Astrophys. J. **910(2)**, 155, 2021.

5) **Dissociative recombination of N_2H^+ ions with electrons in the temperature range of 80–350 K**
Shapko, D., Dohnal, P., Kassayová, M., Kálosi, Á., Rednyk, S., Roučka, Š., Plašil, R., Augustovičová, L. D., Johnsen, R., Špirko, V., Glosík, J.,
J. Chem. Phys. **152(2)**, 024301, 2020.

6) **Towards state selective recombination of H_3^+ under astrophysically relevant conditions**
Dohnal, P., Shapko, D., Kálosi, Á., Kassayová, M., Roučka, Š., Rednyk, S., Plašil, R., Hejduk, M., Glosík, J.,
Faraday Discuss. **217**, 220–234, 2019.

7) **Reaction of NH^+, NH_2^+, and NH_3^+ ions with H_2 at low temperatures**
Rednyk, S., Roučka, Š., Kovalenko, A., Tran, T. D., Dohnal, P., Plašil, R., Glosík, J.,
Astron. Astrophys. **625**, A74, 2019.

8) **Stationary afterglow apparatus with CRDS for study of processes in plasmas from 300 K down to 30 K**
Plašil, R., Dohnal, P., Kálosi, Á., Roučka, Š., Shapko, D., Rednyk, S., Johnsen, R., Glosík, J.,
Rev. Sci. Instrum. **89**, 063116, 2018.

9) **OH^+ Formation in the Low-temperature $O^+(4S)$ + H_2 Reaction**
Kovalenko, A, Tran, T. D., Rednyk, S., Roučka, Š., Dohnal, P., Plašil, R., Gerlich, D., Glosík, J.,
Astrophys. J. **856(2)**, 100, 2018.

10) **Formation of H_2O^+ and H_3O^+ Cations in Reactions of OH^+ and H_2O^+ with H_2: Experimental Studies of the Reaction Rate Coefficients from T = 15 to 300 K**
Tran, T. D., Rednyk, S., Kovalenko, A., Roučka, Š., Dohnal, P., Plašil, R., Gerlich, D., Glosík, J.,
Astrophys. J. **854(1)**, 25, 2018.

11) **Effect of rotational excitation of H_2 on isotopic exchange reaction with OD^- at low temperatures**
Roučka, Š.., Rednyk, S., Kovalenko, A., Tran, T. D., Plašil, R., Kálosi, Á., Dohnal, P., Gerlich, D., Glosík, J.,
Astron. Astrophys. **615**, L6, 2018.

12) **Stationary afterglow measurements of the temperature dependence of the electron–ion recombination rate coefficients of H$_2$D$^+$ and HD$_2^+$ in He/Ar/H$_2$/D$_2$ gas mixtures at T = 80–145 K**

Plašil, R., Dohnal, P., Kálosi, Á., Roučka, Š., Johnsen, R., Glosík, J.,

Plasma Sources Sci. Technol. **26(3)**, 035006, 2017.

13) **Electron-ion recombination in low temperature hydrogen/deuterium plasma**

Glosík, J., Dohnal, P., Kálosi, Á., Augustovičová, L. D., Shapko, D., Roučka, Š., Plašil, R.,

Eur. Phys. J.-Appl. Phys. **80(3)**, 30801, 2017.

14) **Overtone spectroscopy of N$_2$H$^+$ molecular ions—application of cavity ring-down spectroscopy**

Kálosi, A., Dohnal, P., Shapko, D., Roučka, Š., Plašil, R., Johnsen, R., Glosík, J.,

J. Instrum. **12**, C10010, 2017.

15) **Isotopic effects in the interaction of O$^-$ with D$_2$ and H$_2$ at low temperatures**

Plašil, R., Tran, T. D., Roučka, Š., Jusko, P., Mulin, D., Zymak, I., Rednyk, S., Kovalenko, A., Dohnal, P., Glosík, J., Houfek, K., Táborský, J., Čížek, M.,

Phys. Rev. A **96(6)**, 062703, 2017.

16) **Binary and ternary recombination of H$_2$D$^+$ and HD$_2^+$ ions with electrons at 80 K**

Dohnal, P., Kálosi, Á., Plašil, R., Roučka, Š., Kovalenko, A., Rednyk, S., Johnsen, R., Glosík, J.,

Phys. Chem. Chem. Phys. **18(34)**, 23549–23553, 2016.

17) **Monitoring the removal of excited particles in He/Ar/H$_2$ low temperature afterglow plasma at 80–300 K**

Kálosi, Á., Dohnal, P., Augustovičová, L., Roučka, Š., Plašil, R., Glosík, J.,

Eur. Phys. J.-Appl. Phys. **75(2)**, 24707, 2016.

18) **Recombination of H₃⁺ ions with electrons in He/H₂ ambient gas at temperatures from 240 K to 340 K**
Glosik, J; Dohnal, P; Rubovic, P; Kalosi, A; Plasil, R; Roucka, S; Johnsen, R
Plasma Sources Sci. Technol. **24(6)**, 065017, 2015.

19) **Flowing-afterglow study of electron-ion recombination of para–H₃⁺ and ortho–H₃⁺ ions at temperatures from 60 K to 300 K**
Hejduk, M., Dohnal, P., Rubovic, P., Kalosi, A., Plasil, R., Johnsen, R., Glosik, J.,
J. Chem. Phys. **143(4)**, 044303, 2015.

20) **H₂-assisted ternary recombination of H₃⁺ with electrons at 300 K**
Dohnal, P., Rubovic, P., Kalosi, A., Hejduk, M., Plasil, R., Johnsen, R., Glosik., J.,
Phys. Rev. A **90**, 042708, 2014.

21) **Collisional-radiative recombination of Ar⁺ ions with electrons in ambient helium at temperatures from 50 K to 100 K**
Dohnal, P., Rubovic, P., Kotrik, T., Hejduk, M., Plasil, R., Johnsen, R., Glosik, J.,
Phys. Rev. A **87**, 052716, 2013.

22) **Binary Recombination of H₃⁺ and D₃⁺ Ions with Electrons in Plasma at 50–230 K**
Rubovic, P., Dohnal, P., Hejduk, M., Plasil, R., Glosik, J.,
J. Phys. Chem. A **117(39)**, 9626–9632, 2013.

23) **Ternary Recombination of H₃⁺ and D₃⁺ with Electrons in He–H₂ (D₂) Plasmas at Temperatures from 50 to 300 K**
Johnsen, R., Rubovic, P., Dohnal, P., Hejduk, M., Plasil, R., Glosik, J.,
J. Phys. Chem. A **117(39)**, 9477–9485, 2013.

24) **Binary recombination of para- and ortho-H$_3^+$ with electrons at low temperatures**

Dohnal, P., Hejduk, M., Varju, J., Rubovic, P., Roucka, S., Kotrik, T., Plasil, R., Johnsen, R., Glosik, J.,

Philos. Trans. R. Soc. A-Math. Phys. Eng. Sci. **370(1978)**, 5101–5108, 2012.

25) **Binary and ternary recombination of para-H$_3^+$ and ortho-H$_3^+$ with electrons: State selective study at 77–200 K**

Dohnal, P., Hejduk, M., Varju, J., Rubovic, P., Roucka, S., Kotrik, T., Plasil, R., Glosik, J., Johnsen, R.,

J. Chem. Phys. **136(24)**, 244304, 2012.

26) **Binary and ternary recombination of D$_3^+$ ions at 80–130 K: Application of laser absorption spectroscopy**

Dohnal, P., Hejduk, M., Rubovic, P., Varju, J., Roucka, S., Plasil, R., Glosik, J.,

J. Chem. Phys. **137(19)**, 194320, 2012.

27) **Nuclear spin state-resolved cavity ring-down spectroscopy diagnostics of a low-temperature H$_3^+$–dominated plasma**

Hejduk, M., Dohnal, P., Varju, J., Rubovic, P., Plasil, R., Glosik, J.,

Plasma Sources Sci. Technol. **21(2)**, 024002, 2012.

28) **Cryo-FALP study of collisional-radiative recombination of Ar$^+$ ions at 40–200 K**

Kotrik, T., Dohnal, P., Rubovic, P., Plasil, R., Roucka, S., Opanasiuk, S., Glosik, J.,

Eur. Phys. J.-Appl. Phys. **56(2)**, 24011, 2011.

29) **Collisional-radiative recombination Ar$^+$ + e + e: Experimental study at 77–180 K**

Kotrik, T., Dohnal, P., Roucka, S., Jusko, P., Plasil, R., Glosik, J., Johnsen, R.,

Phys. Rev. A **83(3)**, 032720, 2011.

30) **Reactions of Cold Trapped CH⁺ Ions with Slow H Atoms**
Plasil, R., Mehner, T., Dohnal, P., Kotrik, T., Glosik, J., Gerlich, D.,
Astrophys. J. **737(2)**, 60, 2011.

31) **Nuclear Spin Effect on Recombination of H₃⁺ Ions with Electrons at 77 K**
Varju, J., Hejduk, M., Dohnal, P., Jilek, M., Kotrik, T., Plasil, R., Gerlich, D.,
Glosik, J.,
Phys. Rev. Lett. **106(20)**, 203201, 2011.

32) **Temperature dependence of binary and ternary recombination of D₃⁺ ions with electrons**
Kotrik, T., Dohnal, P., Korolov, I., Plasil, R., Roucka, S., Glosik, J.,
Greene, C. H., Kokoouline, V.,
J. Chem. Phys. **133(3)**, 034305, 2010.

33) **Binary and ternary recombination of H₃⁺ and D₃⁺ ions with electrons in low temperature plasma**
Glosik, J., Plasil, R., Kotrik, T., Dohnal, P., Varju, J., Hejduk, M., Korolov,
I., Roucka, S., Kokoouline, V.,
Mol. Phys. **108(17)**, 2253–2264, 2010.

34) **Recombination of HCO⁺ and DCO⁺ ions with electrons**
Korolov, I., Plasil, R., Kotrik, T., Dohnal, P., Glosik, J.,
Int. J. Mass Spectrom. **280(1-3)**, 144–148, 2009.

35) **Non-Maxwellian electron energy distribution function in He, He/Ar, He/Xe/H₂ and He/Xe/D₂ low temperature afterglow plasma**
Plasil, R., Korolov, I., Kotrik, T., Dohnal, P., Bano, G., Donko, Z., Glosik, J.,
Eur. Phys. J. D **54(2)**, 391–398, 2009.

36) **Binary and ternary recombination of D_3^+ ions with electrons in He-D_2 plasma**
Glosik, J., Korolov, I., Plasil, R., Kotrik, T., Dohnal, P., Novotny, O., Varju, J., Roucka, S., Greene, C. H., Kokoouline, V.,
Phys. Rev. A **80(4)**, 042706, 2009.

37) **Temperature dependence of binary and ternary recombination of H_3^+ ions with electrons**
Glosik, J., Plasil, R., Korolov, I., Kotrik, T., Novotny, O., Hlavenka, P., Dohnal, P., Varju, J., Kokoouline, V., Greene, C. H.,
Phys. Rev. A **79(5)**, 052707, 2009.

38) **Measurements of EEDF in Helium Flowing Afterglow at Pressures 500 – 2000 Pa**
Korolov, I., Plasil, R., Kotrik, T., Dohnal, P., Novotny, O., Glosik, J.,
Contrib. Plasma Phys. **48(5-7)**, 461–466, 2008.

Publications in proceedings of scientific conferences listed in WOS

1) **Reactions of O^- with D_2 at temperatures below 300 K**
Plašil, R., Tran, T. D., Roučka, Š., Rednyk, S., Kovalenko, A., Jusko, P., Mulin, D., Zymak, I., Dohnal, P., Glosík, J.,
J. Phys.: Conf. Ser. **875(1)**, 012015, 2017.

2) **State selective study of H_3^+ recombination in Cryo-FALP and SA-CRDS experiments at 77 K**
Glosik, J., Hejduk, M., Dohnal, P., Rubovic, P., Kalosi, A., Plasil, R.,
EPJ Web of Conferences **84**, 01002, 2015.

3) **Recombination in low temperature Ar^+ dominated plasmas**
Dohnal, P., Kotrik, T., Plasil, R., Korolov, I., Glosik, J.,
J. Phys.: Conf. Ser. **300(1)**, 012021, 2011.

4) **Experimental study of para- and ortho-H_3^+ recombination**

   Plasil, R., Varju, J., Hejduk, M., Dohnal, P., Kotrik, T., Glosik, J.,

   J. Phys.: Conf. Ser. **300(1)**, 012023, 2011.

5) **Measurements of EEDF in recombination dominated afterglow plasma**

   Plasil, R., Korolov, I., Kotrik, T., Varju, J., Dohnal, P., Donko, Z., Bano, G., Glosik, J.,

   J. Phys.: Conf. Ser. **192**, 012023, 2009.

6) **Recombination of KrD^+ and KrH^+ ions in afterglow plasma**

   Korolov, I., Kotrik, T., Plasil, R., Hejduk, M., Varju, J., Dohnal, P., Glosik, J.,

   J. Phys.: Conf. Ser. **192**, 012018, 2009.

7) **Recombination of D_3^+ Ions with Electrons in Low Temperature Plasma**

   Korolov, I., Kotrik, T., Dohnal, P., Plasil, R., Glosik, J.,

   Publ. Astron. Obs. Belgrade **84**, 39–44, 2008

Other publications

1) **Equilibrium in Low Temperature H_3^+-dominated Plasma, Application of Cavity Ring-Down Spectroscopy**

   Hejduk, M., Dohnal, P., Rubovic, P., Varju, J., Opanasiuk, S., Plasil, R., Glosik, J.,

   Acta Univ. Carolin. Math. Phys. **53(1)**, 51–59, 2012

List of attached publications

Varju J., Hejduk M., Dohnal P., Jilek M., Kotrík T., Plašil R., Gerlich D., Glosík J.: Nuclear Spin Effect on Recombination of H_3^+ Ions with Electrons at 77 K, *Phys. Rev. Lett.* **106(20)**, 203201, 2011. doi:10.1103/PhysRevLett.106.203201

Dohnal P., Hejduk M., Rubovič P., Varju J., Roučka Š., Plašil R., Glosík J.: Binary and ternary recombination of D_3^+ ions at 80–130 K: Application of laser absorption spectroscopy, *J. Chem. Phys.* **137(19)**, 194320, 2012. doi:10.1063/1.4767396

Dohnal P., Hejduk M., Varju J., Rubovič P., Roučka Š., Kotrík T., Plašil R., Glosík J., Johnsen R.: Binary and ternary recombination of para-H_3^+ and ortho-H_3^+ with electrons: State selective study at 77–200 K, *J. Chem. Phys.* **136(24)**, 244304, 2012. doi:10.1063/1.4730162

Johnsen R., Rubovič P., Dohnal P., Hejduk M., Plašil R., Glosík J.: Ternary Recombination of H_3^+ and D_3^+ with Electrons in He–H_2 (D_2) Plasmas at Temperatures from 50 to 300 K, *J. Phys. Chem. A* **117(39)**, 9477–9485, 2013. doi:10.1021/jp311978n

Rubovič P., Dohnal P., Hejduk M., Plašil R., Glosík J.: Binary Recombination of H_3^+ and D_3^+ Ions with Electrons in Plasma at 50–230 K, *J. Phys. Chem. A* **117(39)**, 9626–9632, 2013. doi:10.1021/jp3123192

Dohnal P., Rubovič P., Kotrík T., Hejduk M., Plašil R., Johnsen R., Glosik J.: Collisional-radiative recombination of Ar^+ ions with electrons in ambient helium at temperatures from 50 K to 100 K, *Phys. Rev. A* **87**, 052716, 2013. doi:10.1103/PhysRevA.87.052716

Dohnal P., Rubovič P., Kálosi A., Hejduk M., Plašil R., Johnsen R., Glosík. J.: H_2-assisted ternary recombination of H_3^+ with electrons at 300 K, *Phys. Rev. A* **90**, 042708, 2014. doi:10.1103/PhysRevA.90.042708

Hejduk M., Dohnal P., Rubovic P., Kálosi Á., Plašil R., Johnsen R., Glosík J.: Flowing-afterglow study of electron-ion recombination of para–H_3^+ and ortho–H_3^+ ions at temperatures from 60 K to 300 K, *J. Chem. Phys.* **143(4)**, 044303, 2015. doi:10.1063/1.4927094

Glosik J., <u>Dohnal P.</u>, Rubovič P., Kálosi Á., Plašil R., Roučka S., Johnsen R.: Recombination of H_3^+ ions with electrons in He/H_2 ambient gas at temperatures from 240 K to 340 K, Plasma Sources Sci. Technol. 24(6), 065017, 2015. doi:10.1088/0963-0252/24/6/065017

Kálosi Á., <u>Dohnal P.</u>, Augustovičová L., Roučka Š., Plašil R., Glosík J.: Monitoring the removal of excited particles in He/Ar/H_2 low temperature afterglow plasma at 80–300 K, *Eur. Phys. J.-Appl. Phys.* **75(2)**, 24707, 2016. doi:10.1051/epjap/2016150587

<u>Dohnal P.</u>, Kálosi Á., Plašil R., Roučka Š., Kovalenko A., Rednyk S., Johnsen R., Glosík J.: Binary and ternary recombination of H_2D^+ and HD_2^+ ions with electrons at 80 K, *Phys. Chem. Chem. Phys.* **18(34)**, 23549, 2016. doi:10.1039/C6CP04152C

Plašil R., <u>Dohnal P.</u>, Kálosi Á., Roučka Š., Johnsen R., Glosík J.: Stationary afterglow measurements of the temperature dependence of the electron–ion recombination rate coefficients of H_2D^+ and HD_2^+ in He/Ar/H_2/D_2 gas mixtures at $T = 80$–145 K, *Plasma Sources Sci. Technol.* **26(3)**, 035006, 2017. doi:10.1088/1361-6595/aa5916

Kálosi A., <u>Dohnal P.</u>, Shapko D., Roučka Š., Plašil R., Johnsen R., Glosík J.: Overtone spectroscopy of N_2H^+ molecular ions—application of cavity ring-down spectroscopy, *J. Instrum.* **12**, C10010, 2017. doi:10.1088/1748-0221/12/10/C10010

Plašil R., <u>Dohnal P.</u>, Kálosi Á., Roučka Š., Shapko D., Rednyk S., Johnsen R., Glosík J.: Stationary afterglow apparatus with CRDS for study of processes in plasmas from 300 K down to 30 K, *Rev. Sci. Instrum.* **89**, 063116, 2018. doi:10.1063/1.5036834

<u>Dohnal P.</u>, Shapko D., Kálosi Á., Kassayová M., Roučka Š., Rednyk S., Plašil R., Hejduk M., Glosík J.: Towards state selective recombination of H_3^+ under astrophysically relevant conditions, *Faraday Discuss.* **217**, 220–234, 2019. doi:10.1039/C8FD00214B

Shapko D., <u>Dohnal P.</u>, Kassayová M., Kálosi Á., Rednyk S., Roučka Š., Plašil R., Augustovičová L. D., Johnsen R., Špirko V., Glosík J.: Dissociative recombination of N_2H^+ ions with electrons in the temperature range of 80–350 K, *J. Chem. Phys.* **152(2)**, 024301, 2020. doi:10.1063/1.5128330

Shapko D., <u>Dohnal P.</u>, Roučka Š., Uvarova L., Kassayová M., Plašil R., Glosík J.: Cavity ring-down spectroscopy study of neon assisted recombination of H_3^+ ions with electrons, *J. Mol. Spectrosc.* **378**, 111450, 2021. doi:10.1016/j.jms.2021.111450

Uvarova L., <u>Dohnal P.</u>, Kassayová M., Saito S., Rednyk S., Roučka Š., Plašil R., Glosík J.: Recombination of vibrationally cold N_2^+ ions with electrons, Prepared for publication in *J. Geophys. Res. Atmos.*

Attached publications